Research paper

Synthesis of new antiproliferative 1,3,4-substituted-pyrrolo[3,2-c]quinoline derivatives, biological and *in silico* insights

Francesco Mingoia [a,*], Caterina Di Sano [b], Claudia D'Anna [b], Marco Fazzari [c], Luigi Minafra [d], Alessia Bono [e], Gabriele La Monica [e], Annamaria Martorana [e], Anna Maria Almerico [e], Antonino Lauria [e]

[a] *Istituto per lo Studio dei Materiali Nanostrutturati - (ISMN) - Consiglio Nazionale delle Ricerche (CNR), Via U. La Malfa 153, 90146, Palermo, Italy*
[b] *Istituto di Farmacologia Traslazionale (IFT) - CNR, Via U. La Malfa 153, 90146, Palermo, Italy*
[c] *Department of Pharmacology and Chemical Biology, University of Pittsburgh, Pittsburgh, PA, 15261, USA*
[d] *Istituto di Bioimmagini e Fisiologia Molecolare - (IBFM) - CNR, C.da Pietrapollastra Pisciotto, 90015, Cefalù, PA, Italy*
[e] *Dipartimento di Scienze e Tecnologie Biologiche, Chimiche e Farmaceutiche (STEBICEF), Sezione di Chimica Farmaceutica e Biologica, Università di Palermo, Viale delle Scienze, Edificio 17, 90128, Palermo, Italy*

ARTICLE INFO

ABSTRACT

A series of biologically unexplored substituted 1,3,4-subtituted-pyrrolo[3,2-c]quinoline derivatives (PQs) was evaluated against a panel of about 60 tumor cells (NCI). Based on the preliminary antiproliferative data, the optimizations efforts permitted us to design and synthesize a new series of derivatives allowing us to individuate a promising hit (**4g**). The insertion of a 4-benzo[d] [1,3]dioxol-5-yl moiety on increased and extended the activity towards five panel tumor cell lines such as leukemia, CNS, melanoma, renal and breast cancer, reaching IG_{50} in the low μM range. Replacement of this latter with a 4-(OH-di-Cl-Ph) group (**4i**) or introduction a Cl-propyl chain in position 1 (**5**), selectively addressed the activity against the entire leukemia sub-panel (CCRF-CEM, K-562, MOLT-4, RPMI-8226, SR). Preliminary biological assays on MCF-7 such as cell cycle, clonogenic assay, ROS content test alongside a comparison of viability between MCF-7 and non-tumorigenic MCF-10 were investigated. Among the main anticancer targets involved in breast cancer, HSP90 and ER receptors were selected for *in silico* studies. Docking analysis revealed a valuable affinity for HSP90 providing structural insights on the binding mode, and useful features for optimization.

1. Introduction

The pyrrolo[3,2-c]quinoline (PQ) scaffold has been known for a long time as a core structure of a many bioactive molecules. In the di-hydro or in the entirely aromatic planar form, this angular tricyclic system continues to attract interest because of multiple activities exhibited. PQs have shown hypotensive properties [1], anti-inamatory and anti-acid responses inhibiting kynurenine-3-hydroxylase [2], and the gastric (H^+/K^+) ATPase proton pump, respectively [3]. Furthermore, PQs behaved as positive allosteric modulators of the muscarinic acetylcholine M4 receptor and, particularly effective for the treatment of neurological and psychiatric disorders associated with dysfunctions of the muscarinic acetylcholine receptor [4]. Other derivatives are helpful for the treatment of latent clinical microorganisms since they are active against Escherichia coli, Enterococcus, Staphylococcus aureus,

Streptococcus, and Mycobacterium tuberculosis [5]. Of note, the introduction of specific chains in the tricyclic system can impart anti-plasmodial in vitro activity with low cytotoxicity, and absence of mitochondrial respiratory inhibition [6]. In some cases, compounds' solubility problems were overcome using salts of the PQ nucleus, obtained by treatment of the structures with strong organic acids. The protonation of basic nitrogen of the molecule has led to water-soluble salts (methanesulfonates) which are relevant in the treatment of microbial infections [7,8]. Recently, several derivatives have shown promising results for the treatment of cognitive disorders associated with Alzheimer's disease [9].

The PQs are also being tested for their potential as more effective and selective anticancer agents. Some authors, consider them to be analogs of the topoisomerase inhibitors camptothecin and netropsin, since they possess possessing valuable antitumor activity against many solid

---

tumors, including breast, ovarian and lung carcinomas [10]. PQ derivatives have also been recognized as novel hedgehog signaling inhibitors [11–13], with appropriate chains added to enhance solubility.

Due to their wide range of activities, the PQ scaffold is versatile and attractive for multi-targeting biological purposes, simply by pharmacophoric modulation with suitable functionalities on the guessed positions. The neutral electron-rich pyrrole portion fused with a basic quinoline moiety makes this tricycle particularly interactive with biological entities. Thus, these premises prompted us to develop a new synthetic access to the PQ skeleton [14], modified and adapted to the new reactants, to evaluate their anticancer potential based on specific decorations.
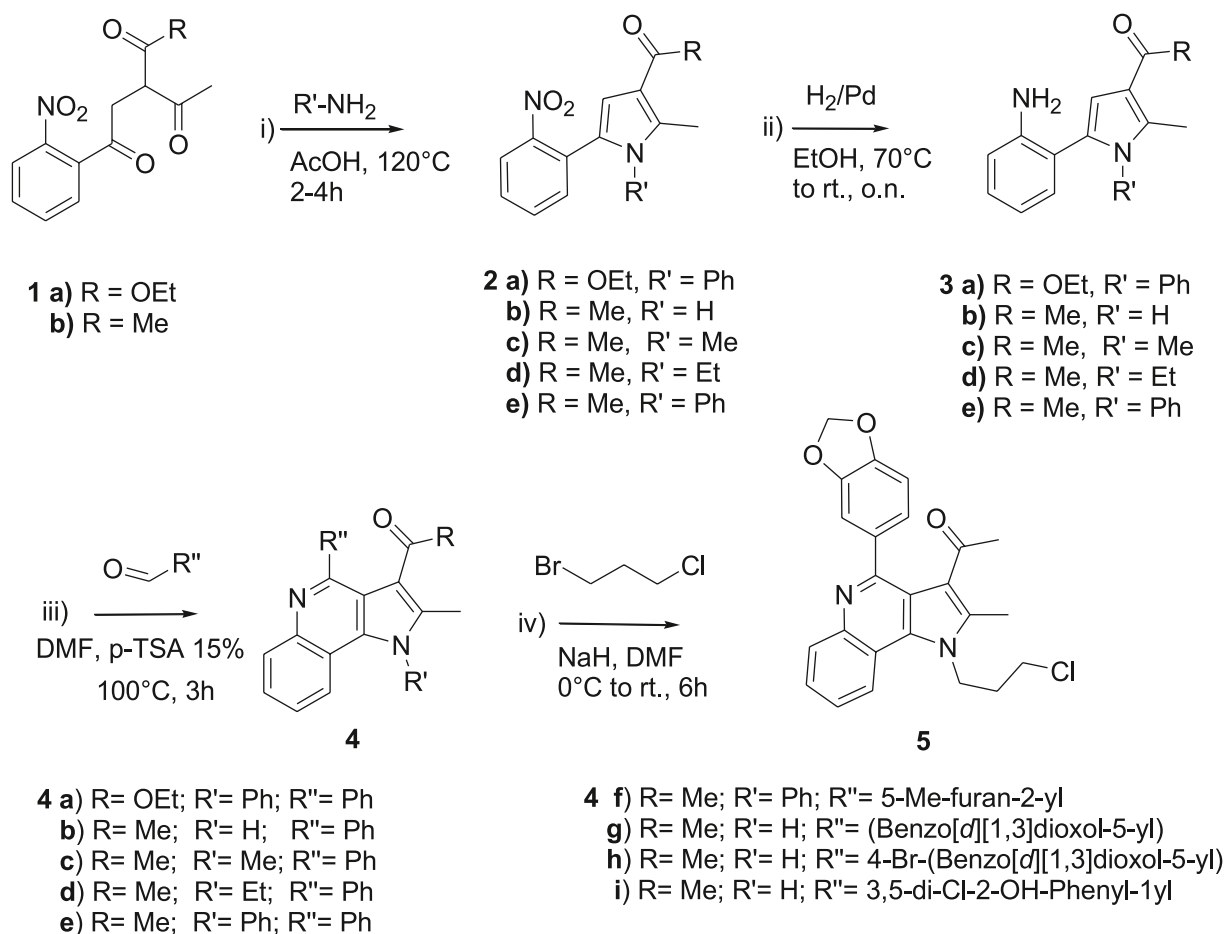
1.1. Synthesis of PQs

The synthetic approach followed herein exploits a previously reported access to the PQ tricycle [14]. The synthesis starts from easily accessible o-nitrophenyl-ketones **1a,b**, which through a formal Paal-Knorr cyclo-condensation in acetic acid with alkyl, aryl, heteroaryl amines afford variously R′ N-linked o-nitro-phenylpyrroles **2** in good to excellent yields. These latter, by classical catalytic reduction procedures

with hydrogen and catalytic Pd/C led to the o-aminophenyl-pyrrole, key intermediates **3**. Further treatment with aromatic or hetero-aromatic aldehydes opens the access, under relatively mild reaction conditions, to a variety of 1-3-4 functionalized pyrrole[3,2-b]quinoline derivatives **4** (PQs). Thus, the pyrrole ring undergoes a sequential intramolecular hetero-annelation of internal imines followed by a spontaneous aromatization of the tricycle.

This synthetic approach is advantageous since it is based on an operationally simple route that uses of a wide range of commercially available alkyl, aryl and heteroaryl amine (step *i*) along with other wide range of commercially available aromatic and hetero-aromatic aldehyde (step *ii*). Features that are crucial for combinatorial like synthesis applications, involving 3 main modulable chemical diversity points, particularly useful for building tailored targeted libraries of compounds. Herein, six biologically unexplored derivatives of the previous series (**4 a-f**) [14] and other newly designed ones (**4 g-i, 5**) were synthesized following the same or modified conditions as reported previously by us and adapting the reaction conditions to the new reactants (Scheme 1).

Furthermore, we introduced on derivative **4g** a Cl-propyl chain in a DMF suspension of NaH at 0 °C to r.t. for 24 h. These experimental conditions also led to the formation of the competitive de-hydro-

i) R′-NH₂, AcOH 120°C, for 2-4h; ii) H₂/Pd on Charcoal, EtOH 70°C to r.t., o.n.
iii) R″CHO, DMF, p-TSA 15%, 100°C for 3h; iv) **4g** treated with NaH in DMFat 0°C to r.t. with 3-Bromo-1-chloropropane, for 24h.
N.B.:Compounds **4a-f** are previously reported [14] but biologically not tested while c.pds **4g-i**, and **5** are newly synthesized.

Scheme 1. Synthesis of pyrrolo[3,2-c]quinoline derivatives (PQ)s selected by NCI.

halogenated compound lowering the yields of the desired compound **5** (yields were not optimized).

All the new PQs derivatives and related intermediates have been characterized by mean of spectroscopic data, ^{1}H NMR e ^{13}C NMR, including IR, GC-MS fragmentation pattern and elemental analysis. All spectral data agreed with the proposed structures.

As a model compound, we report the ^{1}H NMR data of **4g** (Fig. 1). A comparison of the ^{1}H NMR of the precursor *o*-aminophenyl derivative **3b** (R = Me, R' = H) with respect compound **4g**, allowed the confirmation of the occurred cyclization. The disappearance of the amine protons signals at δ 5.02 and the pyrrole ones at δ 6.66 justifies the formation of the angular PQ tricycle. In support of this, we observe a downfield shift of the protons of the neo-formed full aromatic PQ and the up-field proton signals related to the condensed aldehyde. In this particular case, the protons of the (benzo[d] [1,3]dioxol-5-yl)- portion are well distinguishable at more shielded field with respect to aromatic PQ ones (see supplementary material). According to literature reported data and accounting with the effect and position of the substituents, a clear assignment of all signal protons was possible, for derivative **4g**. In the ^{1}H NMR spectra recorded at 400 MHz in DMSO$_{d6}$ the singlet at δ 12.82, exchangeable with D$_2$O, was attributed to the pyrrole N–H. In the most shielded fields, we found two singlets at δ: 2.54 and 1.74, related respectively to 3-acetyl and 2-methyl groups. At δ 6.12, we detect the promptly distinguishable singlet signal due to the benzodioxol methylene.

In the range δ 6.95–7.30 ppm falls the signal of the aromatic benzodioxol protons, easily discernible either for their multiplicity and for their coupling constant. Instead, more deshielded are the signal protons of the pyrrolo[3,2-c]quinoline core. H-6 appears as a doublet with J_o = 6.9 Hz at δ 8.38. It follows a doublet at δ 8.04 with J_o = 7.2 Hz related to proton H-9 that couples with protons H-8 and H-7, which in our case they appear as an apparent multiplet with a coupling constant of a J = 7.2 Hz, confirming the coupling between H-8 e H-9.

1.2. Biological investigations

1.2.1. In vitro cell viability/metabolic assay

A preliminary cell proliferation bioassay (MTS) was carried out by using the CellTiter 96® AQueous One Solution Cell Proliferation Assay (PROMEGA, Madison WI USA), a colorimetric method for determining the number of viable cells in proliferation, cytotoxicity or chemosensitivity [15,16], in five tumor cell lines, (HeLa, cervix; H292, lung; LAN-5, central nervous system (CNS); MCF-7, breast and 16HBE, bronchial epithelial healthy human cell). The antiproliferative profile is listed in Fig. 2.

To decorate the PQ scaffold, we exploited the 3 modular chemical diversity points on position 1,3 and 4 to preliminary evaluate the role of some selected substituents in the antiproliferative activity against the above cited tumor cell lines HeLa, H292, LAN-5, MCF-7, and 16HBE.

NB: Viability data were processed as NCI protocols (see experimental section) and permitted us to highlight either cytostatic activity (**G**rowth **%** (**G%**) or **I**nhibition **G**rowth (**IG**) or **IG$_{50}$**, or **T**otal **G**rowth **I**nhibition
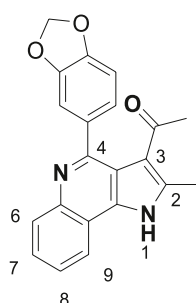

Fig. 1. Derivative **4g**.

TGI$_{50}$), either the cytotoxic activity (Lethal Concentration **LC$_{50}$**) of the tested compounds.

Fig. 2 points out the antiproliferative activity of the substituted PQ skeleton in tumor cell lines, and the role played by the position and nature of the selected functional groups. Notably, LAN-5 and MCF-7 are the two most sensitive tumor cell line to the tested derivatives. Specifically, derivatives **4d,e,f** were active at low concentrations (in the μM range) against LAN-5, while compounds **4b,c,e** were preferentially active against MCF-7. However, the activity in other cell lines (H292, 16HBE, HeLa) was detectable, but with scarce interest.

Among all the derivatives tested so far, compounds **4b** and **4d** were the most promising against the tumor cell lines 16HBE, and LAN5, with a moderate and signficant activity at low concentrations (in the μM range).

Interestingly, the electron-rich nature of the 4-furan-2yl portion (**4f**) and the 1-ethyl moiety (**4d**) seemed to be more active against the CNS cells. When the latter group was replaced with an –H, as in compound **4b,** the activity was slightly moderate in this tumor cell line while it was increased in both MCF-7, 16HBE and moderately in the others.

In summary, compounds **4b** and **4d** were the most active against MCF-7, HeLa, and 16HBE, with an IG50 of 10 μM. Compound **4d** was particularly active and selective showing an IG50 of 1 μM and TGI of 10 μM towards LAN-5. Of note, except for LAN-5, the cytotoxic effect began to appear at concentrations >50 μM. This result is important because it suggests that these derivatives can be used at low dosages without causing severe cytotoxic effects, especially on healthy cells.

1.2.2. In vitro NCI antiproliferative screen

The promising biological in vitro results against five tumor cell lines, encouraged us to submit the first series of compounds (**4a-f**) to the NCI disease-oriented human cell lines screening assay. This assay evaluated for their in vitro antitumor activity a of our compounds against a panel of approximately 60 human tumor cell lines grouped in nine disease subpanels. breast, central nervous system, colon, leukemia, melanoma, non-small cell lung, ovarian, renal, and prostate tumors. The results of NCI screen are shown in Table 1.

The NCI screening validated our previous findings. Once again, derivative **4b,** that was one of the top performers in our cytotoxicity MTS assays, showed interesting low **G%** in the CNS (SNB75, 42%) and Renal subpanel (UO31, 36%; Caki-1 54%). The other derivative **4f,** which has in position 4 of the PQ scaffold an oxygen containing heterocycle (5-Me-Furan-2-yl), showed moderate activity in the Leukemia subpanel, affecting all the cell lines. Moreover, this compound provided a valuable result reaching a **G%** of 41% against the NSCLC subpanel (H226). By replacing the phenyl group of derivative **4e** with a heterocyclic furan one as in **4f**, we observed a 60% of antiproliferative activity against the NSCLC panel (lung) H226 cells, which are generally known for their resistance to chemotherapeutics.

It is to note that, derivative **4b** (containing the 1H-4-Ph group) had a GI of 27% and 16% against the MCF-7 and MDA-MB-231 breast cell lines, respectively. Curiously, when we introduced a second phenyl group (Ph) in position 1, as in derivative **4e** (1,4-di-Ph groups), the trend reversed, and there was a 10% and 24% of GI, respectively. In other words, the activity increased with the introduction of N-1 Ph group towards metastatic cells (MDA-MB-231). Instead, the introduction of a methyl or an ethyl group in position 1 had no effects on both cell lines.

A comparison between derivatives **4a** and **4e**, which have the same substituents in positions 1 and 4 (Ph), suggests that the –COOEt group in position 3 does not significantly affect cell growth.

Overall, these preliminary results confirm that the activity and selectivity depend exclusively on the substituents present in position 1 and 4. In particular, the furan portion is crucial in position 4 for the activity, while for the pyrrole nitrogen the free position (N–H) seems necessary if associated with the 4-Ph. Based on these biologically attracting results, where derivative **4b** and **4f** resulted as the most promising in the 60 NCI tumor panel, we optimized the activity of the
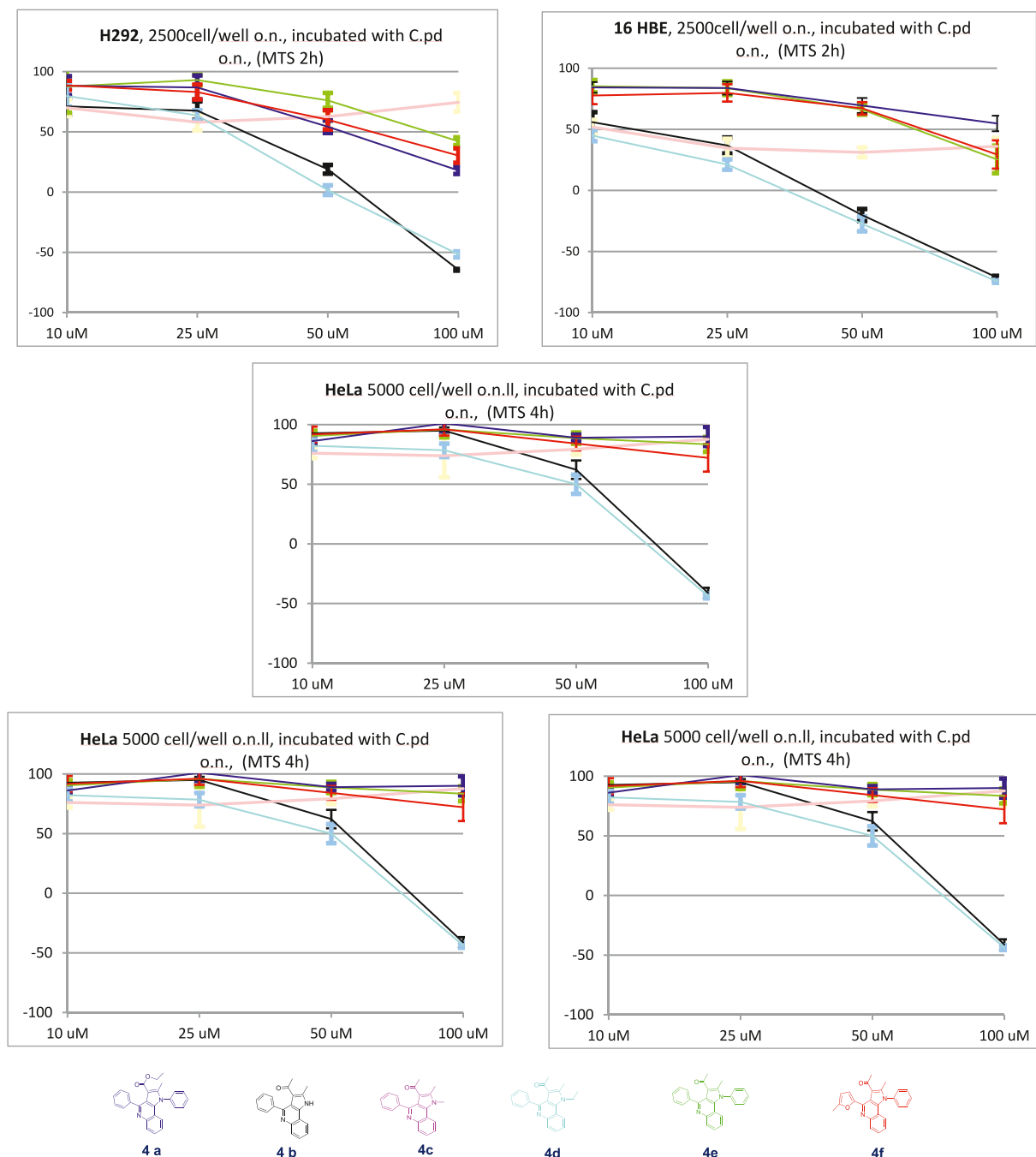
Fig. 2. MTS assays of the first series of synthesized PQs [14]: **4a**, **4b**, **4c**, **4d**, **4e**, **4f**.

PQ derivative by combining the structural parameters/features of the active compounds.

By exploiting our optimized synthetic approach, we synthesized a second series of new derivatives (**4g-i** and **5**) (Schemes 1), and then tested them in the NCI disease-oriented human cell lines screening assay to evaluate their in vitro antiproliferative activity.

Table 2 provides an overview of the results, and the complete data can be found in the Supplementary material. Of note, the new compounds showed improved antiproliferative activity, which was a reward for our design efforts (Table 2).
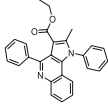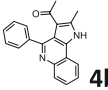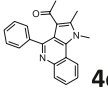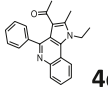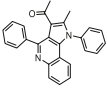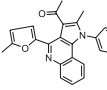
Derivative **4g** showed a much broader range of activity at the concentration of 10 μM targeting five panels such as Leukemia, CNS, Melanoma, Renal and Breast. The introduction of a benzodioxol moiety in position 4 of the PQ core extended the antiproliferative activity against

five tumor cell lines, with mean values ranging from 45 to 60%. However, bromination of this moiety (**4h**), resulted in a loss of activity toward many tumor cells, but not against UO31 renal cancer cells.

The introduction of a Chloro-propyl chain in position 1 provided a valuable selectivity against the leukemia panel, targeting the entire cell lines (K562, MOLT-4, RPMI-820, SR). Interestingly, the same trend was obtained by modifying the substituent at position 4 (derivative **4i** decorated with a di-Chloro-hydroxy-phenyl group).

While some NCI panels (e.g., leukemia) are particularly sensitive to this PQ class of compounds and encourage deeper investigations in the next future, our attention was focused on several selected tumor cell lines (specifically MCF-7), including healthy cells. Our goal was to better understand the mode of action and the chemical features necessary for the design of new more active compounds. Then, we performed several

Table 1

NCI screening of our first series of PQs **4a-f** derivatives (10 μM). Values are expressed as Growth % (**G%**)..

Panel/Cell line	4a	4b	4c	4d	4e	4f
	NSC772322/1	NSC772318/1	NSC772321	NSC772319	NSC772323	NSC772320
Leukemia						
CCRF-CEM	88,8	87,19	92,73	88,48	95,87	**74,18**
HL-60(TB)	89,14	82,68	**76,81**	100,46	90,73	**63,41**
K-562	86,4	92,59	102,19	99,21	**76,81**	**71,63**
MOLT-4	84,26	105,7	89,37	95,22	77,62	**76,67**
RPMI-8226	88,08	87,94	79,37	79,57	87,46	**70,52**
SR	89,86	**71,92**	94,68	91,7	79,45	80,31
NSC Lung Cancer						
NCI-H226	86,98	**76,66**	88,37	**68,31**	84,18	**41,03**
NCI-H522	81,16	**72,34**	95,6	92,64	77,03	**71,07**
Colon Cancer						
HT29	100,38	92,78	111,91	108,32	ND	**68,37**
SNB-75	80,36	**42,3**	85,84	85,13	**75,12**	93,76
Melanoma						
UACC-257	94,71	**75,14**	96,42	93,3	98,07	90,82
UACC-62	**74,67**	**62,38**	87,81	88,93	**70,39**	85,1
RenalCancer						
786-0	85,95	**76,68**	101,32	98,75	88,46	93,6
CAKI-1	91,01	**53,97**	87,21	93,79	**72,27**	85,33
UO-31	80,78	**36,59**	**68,85**	82,52	**59,65**	79,09
Prostate Cancer						
PC-3	**74,46**	78,61	**69,79**	80,5	85,7	**69,58**
Breast Cancer						
MCF7	85,06	**73,67**	95,64	93,56	89,57	88,38
MDA-MB-231/ATCC	**73,44**	84,43	94,3	91,11	**76,35**	**73,29**
T47D	95,87	82,54	98,88	86,95	102,06	99,68
Mean	94	86,68	97,49	97,73	88,31	87,84
Delta	20,56	50,09	28,64	29,42	28,66	46,81
Range	54,1	76,5	50,05	51,87	61,32	67,25

blue value indicates moderate antiproliferative activity (range ≈ 25-30% of growth inhibition GI at 10 mM).
red value means interesting to good antiproliferative activity (range ≈ 30-75% of GI) at 10 mM.
N.B. The trend preliminary observed by us for derivative **4b** was further confirmed by the NCI screening. Complete NCI panels are available in the Supplementary Material, here are reported only those with one score almost down 75 G%, except for T47D cell which was inserted for comparative reasons. For complete G% value consult NCI web site and search with NSC number.

biological investigations on the identified "hit", derivative **4g**.

1.2.3. Effects of 4 g on cell cycle events in MCF-7

MCF-7 cell line was cultured for 72 h with derivative **4g** at 5, 10, 15 and 25 μM and cell cycle perturbation was assessed (Fig. 3). M1 (apoptosis zone, red color) was significantly increased at 5 and 10 μM. Instead, along the increase in concentration treatments (5, 10 and 25 μM), a dose dependent decrease of M2 (grey color) was observed. The more evident effect appeared at 25 μM, where derivative **4g** was able to increase significantly M3 zone (green color) related to S phase. Curiously, M4 (blue color G2/M phase) was moderately decreased at a lower dose (5 μM), beside a slight increase at higher doses (10 and 25 μM).
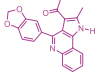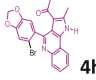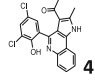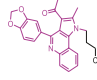
The dose of compound **4g** had a significant impact on cell cycle distribution (Fig. 3). At the low dose (5 μM) there was a substantial increase of the M1 zone, which is typically associated with apoptotic cells. However, when we doubled the dosage, the response was not proportionally correlated. At a higher dose of 25 μM, the most relevant increase in cell distribution concerned mainly the S phase, while the SubG1 phase (apoptotic) decreased considerably.

1.2.4. Cell colony assay of MCF-7 cells treated with 4 g

MCF7 cell line was cultured for 72 h with **4g** (at 5, 10, 15 and 25 μM)

Table 2
Overview of the NCI one dose Mean Graph of the new derivatives **4g-i, 5**..

Tumor Panel	Cell line	4g NSC752654/1	4h NSC798078/1	4i NSC798083/1	5 NSC798088/1
Leukemia	CCRF-CEM	ND	92	**58,21**	77,14
	K-562	**76,18**	85,21	**74,80**	**71,03**
	MOLT-4	106,96	83,85	**51,62**	**67,31**
	RPMI-8226	90,29	96,91	**66,68**	83,3
	SR	**31,64**	**73,99**	**52,23**	**53,08**
Non-Small Cell Lung Cancer (NSCLC)	A549/ATCC	81,66	88,73	83,54	81,72
	EKVX	88,27	89,61	**72,82**	85,97
	HOP-62	**67,47**	91,47	79,9	96,95
	NCI-H226	**65,58**	99,66	87,42	114,76
	NCI-H522	100,78	77,01	**69,98**	**63,69**
Colon Cancer	HCT-116	84,32	98,88	**75,16**	93,59
	HCT-15	**69,48**	97,2	**73,12**	86,95
	KM12	**74,64**	90,95	**75,12**	87,33
CNS Cancer	SF-295	91,09	94,19	**74,13**	76,71
	SNB-75	**46,47**	84,01	**72,78**	**69,36**
Melanoma	LOX IMVI	86,51	89,31	**73,59**	90,03
	MDA-MB-435	**42,11**	95,57	85,57	93,64
	UACC-257	**73,9**	105,27	117,78	102,34
Ovarian Cancer	IGROV1	**60,08**	82,55	**75,63**	93,89
	SK-OV-3	88,79	96,67	**75,22**	97,21
Renal Cancer	ACHN	92,4	92,99	**71,25**	84,41
	CAKI-1	**58,85**	95,59	77,58	86,68
	UO-31	**26,43**	**61,5**	**56,83**	85,41
Prostate Cancer	PC-3	**75,78**	85,52	**71,39**	**76,15**
Breast Cancer	MCF7	**41,5**	**70,21**	**73,96**	83,21
	MDA-MB-231/ATCC	82,23	88,19	**71,97**	95,83
	T-47D	**70,29**	91,36	**61,91**	**71,48**
	MDA-MB-468	**59,47**	109,23	89,73	100,78
	Mean	82,99	94,42	81,37	90,98
	Delta	56,56	32,92	29,75	37,9
	Range	98,37	58,74	66,16	61,68

NCI Biological Sulforhodamine B based protocol [17]. Results for each tested compound are reported as the percent of growth (G%) of the treated cells when compared to the untreated control cells.
N.B: **blue value** means antiproliferative activity (25-30% GI), **red value** means antiproliferative activity (range 30-75% GI).
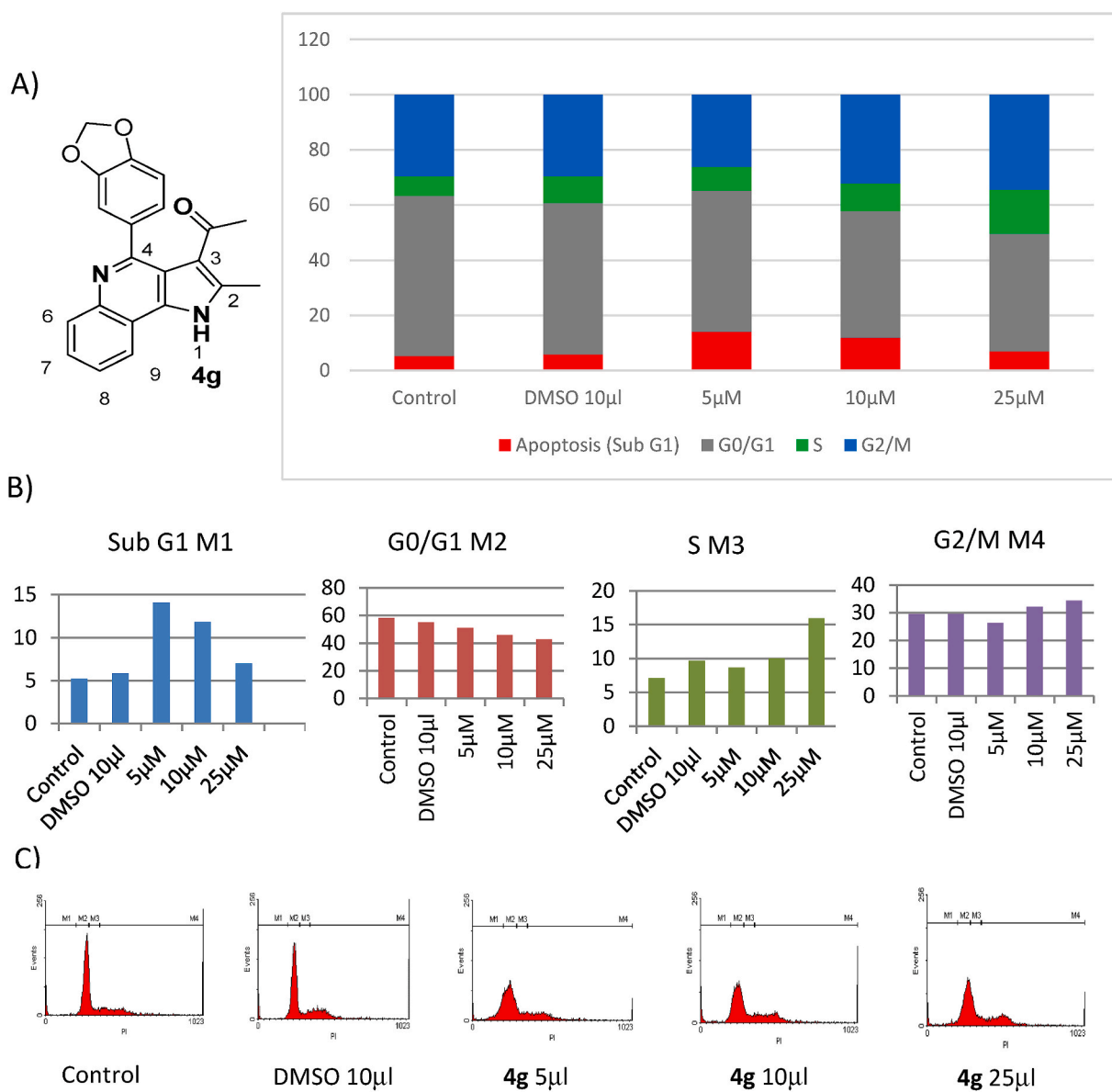
Fig. 3. Effect of **4g** in cell cycle events (MCF-7). **A, B)** Interaction BAR Plot for M1 (apoptosis Sub G1), M2 (Go/G1), M3 (S phase) and M4 (G2/M) Results are expressed as mean ± SD (n = 3). The comparison between different experimental conditions was evaluated by ANOVA corrected with Fisher's test. *p < 0,05 was accepted as statistically significant. (* *vs untreated*; ** *vs DMSO*). **C)** Cytofluorimetric plots of **4g** effect in cell cycle events (MCF-7).

and colony forming ability was assessed by clonogenic assay. A significant reduction in colony number was observed upon exposure of **4g** at all the tested concentrations, in a dose dependent manner (Fig. 4).

1.2.5. ROS content in MCF-7 cell lines treated with 4 g

At all the tested concentrations, a significant increase in ROS levels was observed upon exposure of **4g** (Fig. 5).

1.2.6. Comparative effects on cell viability of 4 g on breast cancer cell lines

To better understand how derivative **4g**, affected cell proliferation, in vitro cell viability studies were performed on two breast cancer (BC) cell lines: (MCF-7 and the metastatic MDA-MB-231) and one non-tumorigenic mammary epithelial cell line (MCF-10A). The first two cell lines were chosen because they represent different levels of tumor aggressiveness while the last one retains a healthy proliferative pattern.

To analyze the cellular response of the pharmacological treatments at the level of cell reproductive capacity rather than on an indirect metabolic level, (as in the MTS cell proliferation assay), a cell counting

was performed (Fig. 6) [18,19].

At a concentration of 10 μM, derivative **4g** inhibited cell growth capacity in both BC cell lines, after 24 h of treatment, with a similar trend: a 32% and a 37% inhibition in MCF-7 and MDA-MB-231 cells respectively. However, after 72 h, the growth inhibition effect was decreased, suggesting that the cells partially recovered from the toxic effects. This trend was more evident in the MDA-MB-231 cells, where growth inhibition decreased to 25%, while the MCF-7 showed values comparable to those observed at 24 h (28%).

At higher concentrations of 25 and 50 μM, there was an increase in growth inhibition in both cell lines after 24 h of treatment (GI: 38% and 54% in the MCF-7 cells and 48% and 60% in the MDA-MD-231, respectively). After 72 h of treatment, a further increase of growth inhibition in MCF7 cells was observed (GI: 41% and 70%). At the same time point in MDA-MB-231 cells, GI increased to 74% and decreased to 35% at 50 and 25 μM respectively.

On the contrary, in the non-tumorigenic MCF-10A cells, the growth inhibition capacity induced by **4g** at the concentration of 10 μM was
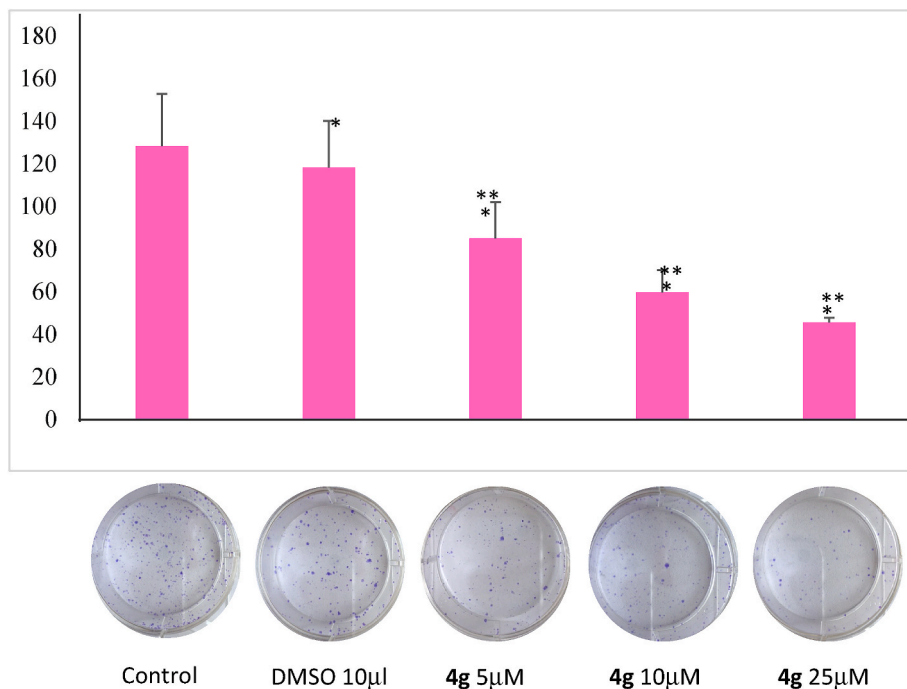
Fig. 4. Clonogenic assay. Effect of **4g** at different concentration on colony formation ability in MCF7 cell line. Results are expressed as mean $\pm$ SD (n = 3). The comparison between different experimental conditions was evaluated by ANOVA corrected with Fisher's test. *p < 0,05 was accepted as statistically significant.
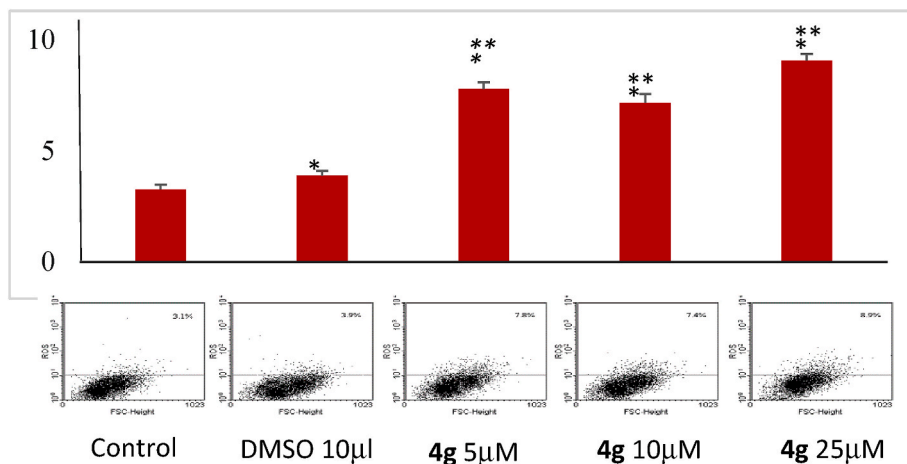
Fig. 5. ROS content in MCF-7 cell line. Results are expressed as mean $\pm$ SD (n = 3). The comparison between different experimental conditions was evaluated by ANOVA corrected with Fisher's test. *p < 0,05 was accepted as statistically significant. * *vs untreated; ** vs DMSO.*
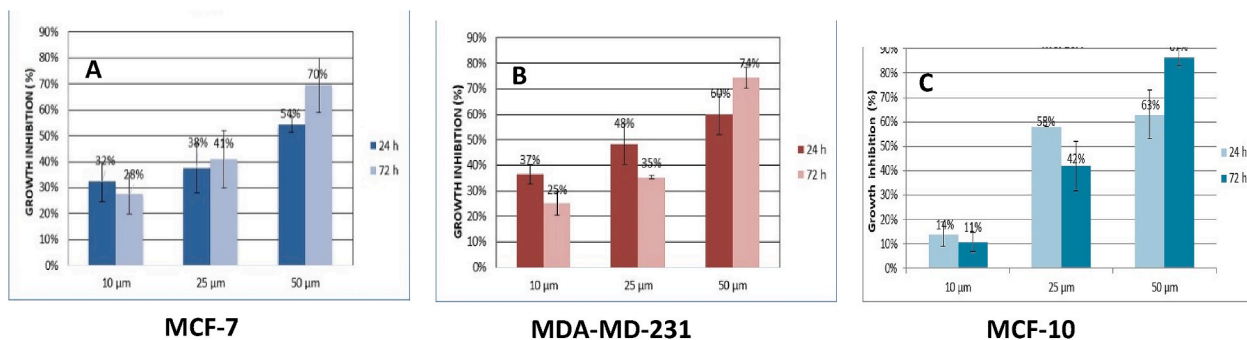
Fig. 6. Cell proliferation assay after treatment with the derivative **4g** at increasing concentrations of 10, 25 and 50 μM against the MCF-7 **(A),** MDA-MD-231 **(B)** and MCF-10A **(C)** BC cell lines. Cell growth inhibition is expressed in percentage with respect to the cell number of each untreated sample used as control.

significantly lower at 24 and 72 h in comparison with the two BC cell lines, with values of 14% and 11% respectively. Therefore, this data indicates that the derivative **4g** at the lowest concentration resulted less toxic against healthy cell. However, at higher concentrations (25 and 50 μM) and both time points, the GI increased and became comparable to the other BC cell lines (GI: 58%–42% at 25 μM and 63%–87% at 50 μM). These results suggest that although MCF-10A is a non-tumorigenic cell line, it is immortalized and, when exposed to high concentrations of **4g**, may activate cell survival mechanisms like those of tumor cell lines.

2. Computational insights: virtual screening on ER & HSP90 Receptors, key targets for MCF-7 cells proliferation

Estrogen receptor (ER) and the 90 KDa Heat Shock protein (HSP90) play important roles in regulating several key biological functions (modulation of gene transcription, cell signaling, proliferation and survival), making them excellent targets for cancer therapy [20–23]. Both ER and HSP90 proteins have been shown to be overexpressed or constitutively more active in cancer cells. In the MCF-7 cell line, they play a critical role in maintaining breast cancer cells proliferation [24, 25]. Therefore, simultaneously targeting these two proteins represents an effective strategy for the therapeutic treatments of cancer. In view of these considerations, *in silico* ligand and structure-based protocols, were performed against the targets ER and HSP90, to identify selective inhibitors for both proteins.

2.1. In silico ligand-based approach: Biotarget Predictor Tool (BPT)

The synthesized structures were analyzed using the Biotarget Predictor Tool (BPT), a ligand-based protocol implemented in DRUDIT[ONLINE] (www.drudit.com) [26], a free web-service based on the calculation of molecular descriptors by MOLDESTO (MOLecular DEScriptors TOol). According to the BPT, the prediction of the affinity of the input structures for the selected biological targets, ER and HSP90, was evaluated via DRUDIT Affinity Score (DAS), a parameter whose values (in the range 0 ÷ 1, low ÷ high affinity) were calculated using the standard DRUDIT parameters (N = 500, Z = 50, G = a).

Table 3 shows the values of DAS for each input molecules versus ER and HSP90 proteins. In general, all the selected compounds exhibited good affinity for both HSP90 (with DAS > −0,648) and ER (with DAS > −0,502) targets. In detail, compound **4g** proved to be the most interesting of the series, with the highest affinity for HSP90 (DAS = −0, 818), even in its salt form **4g**[(+)] (DAS = 0,-76), and moderate affinity for ER (DAS values of = −0,648 and −0,638, for **4g** and **4g**[(+)], respectively). The analysis of these encouraging preliminary ligand based data prompted us to plan further investigations with structure-based studies in the second step of the *in silico* analysis.

Table 3
BIOTARGET *Drudit Affinity Score* for the compounds **4a-i** and **5**.

Compound	HSP90	ER (Estrogen Receptor)
4a	0.612	0.499
4b	0.658	**0.726**
4c	0.648	0.620
4d	0.666	0.540
4e	0.700	0.506
4f	0.718	0.502
4g	0.818	0.648
4g[(+)]	**0.776**	**0.638**
4h	0.666	0.526
4h[(+)]	0.714	0.526
4i	0.744	0.586
5	0.790	0.526
5[(+)]	0.768	0.510

N.B: Sign "(+)" refers to a positively charged form of the molecule at physiological pH range.

2.2. In silico structure-based studies: Molecular Docking at both binding sites of HSP90 and ER proteins

Induced Fit Docking (IFD) studies were performed to gain additional insight into the structural features of ligand/protein complexes and the binding mode of the selected hits. Thus, Molecular Docking simulations were used to analyze the selected molecules within the two selected targets, using PDB IDs 5GGZ [27] and 2EWP [28], for HSP90 and ER, respectively.

2.2.1. In silico structure-based studies: Molecular Docking at the HSP90 binding site

Hsp90 is organized into three domains: an *N*-Terminal adenosine triphosphate/adenosine diphosphate (ATP/ADP) binding domain (NTD); a central region, involved in client protein binding, and a *C*-Terminal Domain (CTD), which is involved in the dimerization process [27]. The NTD possess a two-layered α/β sandwich structure (Fig. 7a), in which the helices delimit a pocket extending from the protein surface to the buried face of the highly twisted antiparallel β-sheet, identifying key conserved functional residues.

In details, NTD includes a conserved solvent area and a hydrophobic sub pocket, consisting of Leu[107], Phe[138], Val[150], and Val[186] (Fig. 7b), which could be occupied by hydrophobic groups, improving affinity [27] to HSP90.

Induced Fit Docking analysis was performed to investigate the capability of the synthesized small molecules to complex the ATP-binding site of HSP90. Table 4 shows the Prime Energy, IFD and docking scores of the compounds **4a-f**, **4g-i** and **5**.

The IFD analysis confirmed the results of the previous ligand-based studies (all derivatives showed interesting IFD scores, in the range −418.804 to −414.127). This trend accounts for the capability of all the tested compounds to deeply penetrate the ATP binding pocket of HSP90. As shown in Fig. 8a, the ligands **4c-f** overlaps perfectly in the binding pocket with a redundancy in the position of the structural key moieties of the molecules within the site, characterized by a large number of interactions. The PQ substituted scaffold is capable to penetrate deeply into the hydrophobic sub-pocket (Leu[107], Phe[138], Val[150], Val[186]), and stabilizes the ligand/protein complex with π−π staking interactions with Phe[138]. The carbonyl moiety and the furane ring (in the case of compound **4f**) form a tight network of hydrogen bonds with residues Asp[93], Thr[184], and conserved water molecules, which anchor the compound into the ATP pocket.

In Fig. 8b is shown the 3D HSP90 ATP-binding pocket in complex with **4g**, which, similarly, to compounds **4c-f**, fits into the hydrophobic sub-pocket with its PQ substituted scaffold and exposes its benzodioxol moiety in the solvent area.

2.2.2. In silico structure-based studies: Molecular Docking at the ER binding site

The estrogen receptor possesses three distinct functional domains: the transactivation function domain, the DNA binding domain, and the Ligand Binding Domain (LBD). The LBD is a three-layer α-helix sandwich with a relatively large cavity (Fig. 9) [28]. The main receptor interactions are the hydrogen binds, involving the backbone and/or side chain of polar amino acids around the binding site, accomplished by the non-polar hydrophobic interaction of the rest of the structure.

Docking analysis aimed to explore the capability of the synthetized small molecules to occupy the ER LBD were performed. Table 5 shows the Prime Energy, IFD and docking scores of the structures **4a-f**, **4g-i** and **5**.

A significant number of interactions were observed between the PQ ligands and the receptor, indicating a high affinity for the ER LBD. Compound **4g** (IFD score −457,026) is anchored into the binding pocket, forming many stabilizing interactions (in Fig. 10a the 3D binding mode of **4g** in the binding pocket is shown, while in Fig. 10b the 2D interaction diagram is reported): the PQ scaffold creates π-π stacking
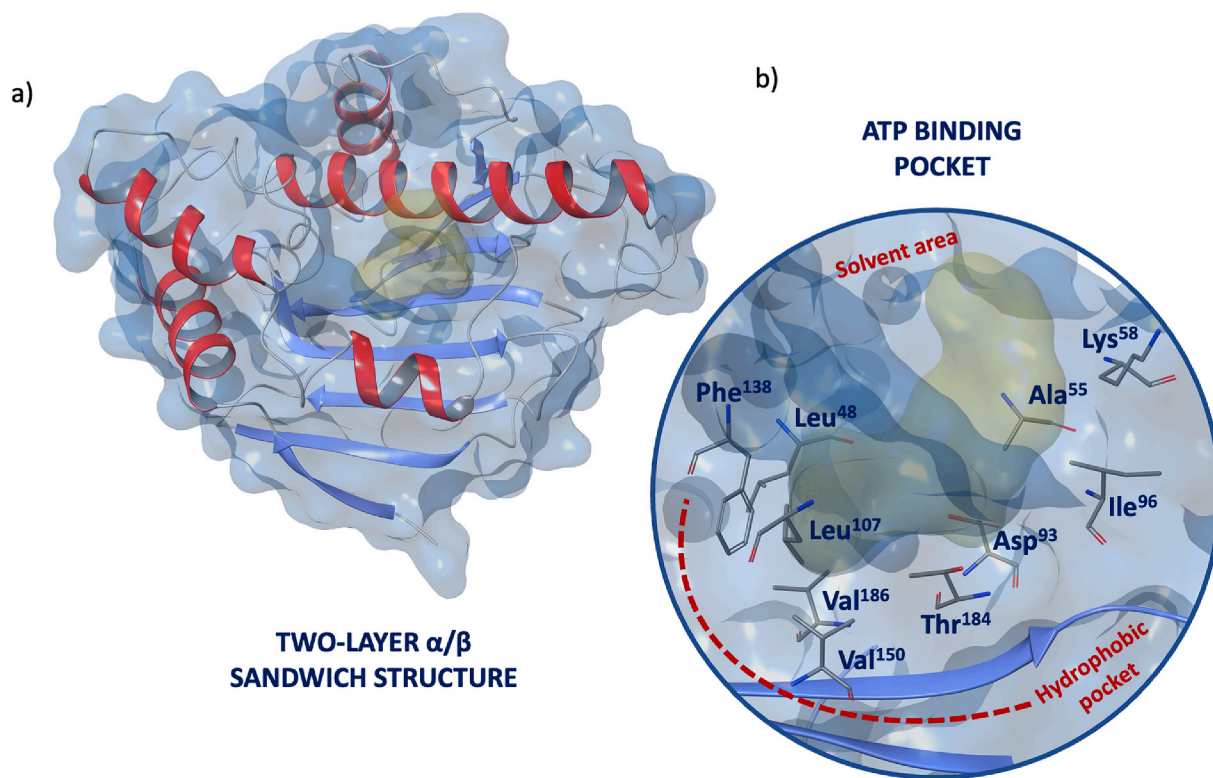
Fig. 7. (**a**) X-Ray structure of two-layer α/β sandwich structure of HSP90 ATP binding pocket (PDB ID: 5GGZ) [27]; (**b**) focus on the ATP binding site, highlighting key conserved functional residues of the hydrophobic pocket and the solvent area (PDB ID: 5GGZ) [27].

Table 4
Prime Energy, XP and IFD scores for structures **4a-f**, **4g-i** and **5** (PDB ID: 5GGZ).

PDB ID: 5GGZ			
Compound	Prime Energy	XP GScore	IFD Score
4f	−8135	−12.055	−418.804
5[(+)]	−8134	−10.977	−417.676
4h	−8158.5	−8.909	−416.832
4e	−8110.6	−11.298	−416.83
4a	−8156.66	−8.545	−416.61
5	−8154.6	−8.67	−416.4
4g[(+)]	−8147.1	−8.574	−415.931
4b	−8136	−9.101	−415.899
4g	−8158.9	−7.943	−415.888
4d	−8126.4	−9.347	−415.665
4h[(+)]	−8138.6	−8.371	−415.303
4i	−8140.9	−7.698	−414.744
4c	−8105.9	−8.833	−414.127

N.B.: Sign "(+)" refers to a positively charged form of the molecule at physiological pH range.

interactions with the side chain of Tyr[326], anchoring the ligand into the pocket and allowing for the formation of reinforcing hydrogen bonds between the hydroxyl group of Tyr[326] and the carbonyl oxygen of **4g**, as well as the imidazole ring of His[434] and the benzodioxole of **4g**.

2.3. ADME parameters calculation

In the design of new small molecules endowed with biological activities, the evaluation of chemical and pharmacokinetics properties is a key aspect to be considered, already in the early stage of the drug discovery pipeline. In this light, we exploited the well-established SwissADME web [29] tool (freely accessible at http://www.swissadme.ch) to predict rapidly key parameters, such as water solubility, pharmacokinetics parameters, drug-likeness, and medicinal chemistry friendliness

for the collected hits. In detail, the majority of compound exhibited optimal values of predicted logP, moderate water solubility (ESOL [30] and Ali Class) [31], and capability to be highly absorbed in the gastrointestinal trait (ideal for oral administration). Furthermore, regarding the lead and drug-like properties, PAINS filters [32], Lipinski's rule (the pioneer rule-of-five) [33], Veber rules [34], and Egan rules [35] were examined to verify compounds drug-likeness, showing that all the selected structures have no violations and no PAINS.

3. Discussion

We report the structure-activity relationship against tumor cell lines of a two series of PQ derivatives synthesized using an optimized approach that allowed an easy introduction of functionalities in few steps, particularly on position 1 and 4 of the PQ scaffold. In a preliminary evaluation (MTS), the first series of compounds showed promising antiproliferative activity against five tumor cell lines (HeLa, H292, LAN-5, 16HBE, MCF-7), indicating their potential as anticancer agents. To further explore their selectivity and potency, we screened them against an NCI tumor panel of approximately 60 human tumor cell lines. Based on these results, we identified a compound with the best outcome and planned to develop it further designing and synthesizing a second series of new suitably decorated derivatives to be tested by NCI against the already mentioned tumor panel. The best result was obtained by introducing a benzodioxol portion in position 4 of the PQ scaffold (compound **4g**), which was selective against five different NCI tumor panels (Leukemia, CNS, Melanoma, Renal and Breast) at low concentration range (10 μM). This unique selectivity pattern may suggest a common cell pathway involved in the compound's mechanism of action, which needs further clarification. Interestingly, attaching a Chloropropyl chain in position 1 or replacing the benzodioxol group with a di-Chloro-hydroxy-Phenyl disrupted this selectivity pattern but resulted in a remarkable selectivity against the entire Leukemia panel (K562, MOLT-4, RPMI-820, SR). Moreover, although moderate, our newly
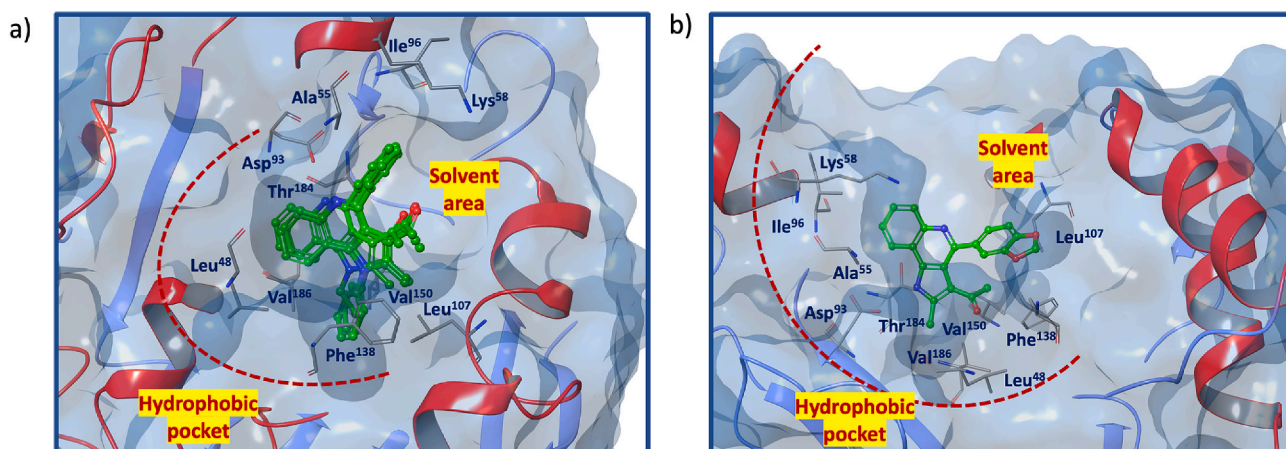
Fig. 8. (**a**) 3D overlaps of compounds **4c-f** in the HSP90 ATP binding site (PDB ID: 5GGZ); (**b**) 3D complex of compounds **4g** in the HSP90 ATP binding site (PDB ID: 5GGZ).
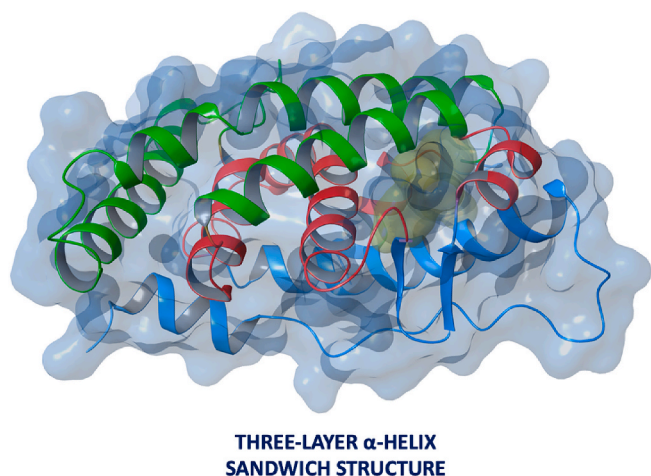

Fig. 9. X-Ray structure of three-layer α-helix sandwich structure of ER ligand binding pocket (PDB ID: 2EWP) [28].

Table 5
Prime Energy, XP and IFD scores analysis for structures **4a-f**, **4g-i** and **5** (PDB ID: 2EWP) [28].

PDB ID: 2EWP			
Compound	Prime Energy	XP GScore	IFD Score
5[(+)]	−8944.4	−11.503	−458.725
4g	−8877.7	**−13.142**	−457.026
4g[(+)]	−8915.0	−11.204	−456.956
5	−8879.8	−12.825	−456.814
4h[(+)]	−8932.5	−9.3632	−455.988
4f	−8888.2	−10.798	−455.207
4i	−8876.7	−10.699	−454.536
4h	−8851.6	−11.631	−454.215
4c	−8853.2	−10.717	−453.377
4e	−8835.7	−11.543	−453.335
4d	−8831.5	−11.427	−453.001
4b	−8843.4	−10.802	−452.972
4a	−8861.6	−9.3662	−452.447

N.B: Sign "+" refers to a protonated form of the molecule at physiological pH range.

designed derivatives showed a more interesting activity against the breast sub-type T47D [36]. Comparing data of Table 1 and related to T47D cells, compounds **4d**, **4i** and **5** showed promising sensibility towards such a cell type. This result constitutes a good basis for future

studies.

Accordingly, further biological investigations aimed to get insights on how these antiproliferative PQ derivatives could really act in the cell context have been achieved. Thus, a cell cycle perturbation was achieved on MCF-7 cells. Other than the interesting antiproliferative property, compound **4g**, exhibited at low concentration significant apoptotic induction along with a cell cycle perturbation in S phase, testified by the increase of cell distribution in M3 cytofluorimetric area, while no substantial variation in M2 and M4 was observed. This data could suggest a main effect in which DNA and related enzymes are particularly active.

In addition, to get information on the capability of a single cell to form a colony and to test for the effects of drugs on the growth and proliferative characteristics of cells in vitro, a clonogenic assay was performed [37]. Clonogenic assays serve as a useful tool to test whether a given anticancer drug can reduce the clonogenic survival of tumor cells. Only a fraction of seeded cells retains the capacity to produce colonies [38]. Our assays confirmed that compound **4g** after the insult imparted on the MCF-7 cells, the colonies were consistently reduced in a dose dependent manner (Fig. 4).

Furthermore, because of ROS are reactive species capable of causing damage to biomolecules, including proteins, lipids, and nucleic acids, leading to cell and tissue injury, such properties are warmly welcomed for cancer cells. Indeed, if the levels of ROS significantly overwhelm the capacity of antioxidant defenses, a potential damage in a biological system could arise and usually causes cell death (e.g., oncosis, apoptosis, and autophagy) [39]. In our case, as shown in Fig. 5, barely at the lower concentration (5 μM), upon exposure of **4g**, a significant increase in ROS levels was observed. This data could be related with the observed apoptotic induction at the same dosage.

Moreover, we compared the viability of the three breast cells, one of which tumorigenic (MCF-7), one metastatic (MDA-MD-231) and one healthy (MCF-10), by treatment with **4g**. At the lower dose (5 μM), the healthy cell resulted less affected with respect the others. At higher doses, the trend appeared differently, overlapping with the trend typical of the tumorigenic cell. The human epithelial MCF10A cell line is commonly used for in vitro studies as the counterpart of healthy breast tissue. However, this cell line although non tumorigenic is immortalized and exhibits some molecular and growth traits similar to breast cancer cell lines. These features could explain the growth behavior of MCF10A cells in response to higher concentrations of **4g** comparable to that observed in the other two mammary cancer cell lines". Other evidence concerns an observed slight increase in the growth inhibition towards metastatic cells compared to the others.

Lastly, the *in silico* studies, including both ligand and structure-based approaches, confirmed the capability of the best-scored compound **4g**,
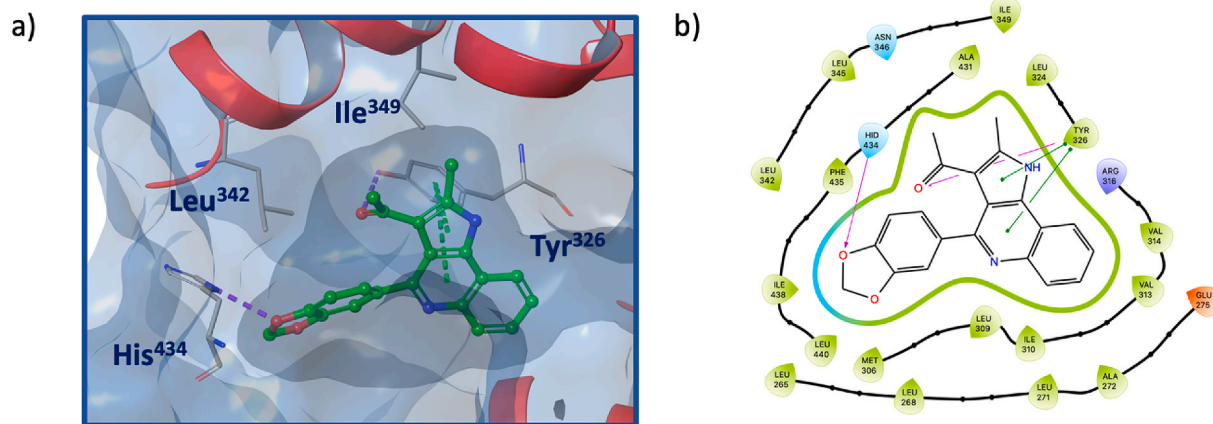
Fig. 10. (a) Predicted 3D binding modes of compounds **4g** into the ER LBD (PDB ID: 2EWP) [28]; **(b)** ligand-protein interaction diagram for **4g**. Hydrogen bonds in violet, while the π-π stackings interactions are shown in green.

to modulate HSP90 and ER receptors, pointing out it as a promising strategy in anticancer therapies. The prediction of the affinity of the input structures for the selected ER and HSP90 biological targets, performed with ligand-based protocol implemented in the web service DRUDIT, has evidenced for the compound **4g** the highest affinity either in neutral or protonated forms towards HSP90, while the affinity towards ER, although moderate, remains in any case of interest. Further *in silico* refinements, involving IFD studies on the specific HSP90 ATP-binding site (PDB ID: 5GGZ) confirmed the previous ligand-based results in which the PQ scaffold can bind into the hydrophobic sub pocket by forming various interactions with the key amino acids in the binding (Fig. 8a). Particularly, derivative **4g**, the more active one, by a slight rotation has exposed its hydrophilic benzodioxol moiety in the solvent area (Fig. 8b). Moving to the ER LBD, to a lesser extent, also the PQ ligands showed a significant number of interactions (Fig. 10a) anchoring the ligand into the pocket and allowing for the formation of reinforcing hydrogen bonds. The carbonyl oxygen, the benzodioxol portion, and the PQ skeleton of **4g**, seem to be the best for the better interaction.

4. Conclusions

By exploiting our previous optimized synthetic approach that allows an easy introduction of functionalities on strategical positions into the PQ scaffold, it was possible the individuation of new promising anti-proliferative agents by a combined empirical and *in silico* support. In summary, a low dose of the hit **4g** induces apoptosis in MCF-7 and a comparison with healthy MCF-10, highlights lower cell damage. In this regard, further studies to assess the safety of **4g** are needed to support the use of this molecule as candidate for cancer therapy. Doubling the dose, a substantial increase on S phase cell events is observed while the effect against all breast cells becomes similar, but revealing more promising towards T47D breast cancer cells. Thus, the structural features of **4g** highlight how the 4-benzodioxol coupled with the N–1H, are the right assembled groups that "make the difference" with respect the others, possessing the properties which suitably balance the crucial hydrophobic/hydrophilic interactions into our investigated receptors.

These preliminary results allow us to lay the foundations for the design of new derivatives for the optimization of new active molecules against several tumor panels. *In silico* studies showed as the identified compounds can be considered an excellent starting point for the design of new hits able to modulate the carcinogenic pathways involved in breast cancer and, targeting HSP90 and ER receptors with ADME predictions that support their potential application as possible drug candidate.

5. Experimental section

5.1. Chemistry. Synthesis and characterization

Reagents and reactants were purchased from commercial suppliers (Aldrich) and used without further purification. DMF was distilled under vacuum prior treatment by CaH_2. Analytical thin layer chromatography was performed on Merck precoated silica gel (60F254) plates and column chromatography on Merck silica gel 230–400 mesh (ASTM). Melting points were determined with a Sanyo-Gallenkamp capillary apparatus and are uncorrected. IR spectra were recorded in bromoform with a Jasco FT-IR 5300 spectrometer. ^{13}C NMR spectra were recorded on a Bruker AC 250 spectrometer operating in FT mode in DMSO-d_6 solutions at 250.13 and 62.89 MHz, respectively. ^1H and ^{13}C chemical shift values are given in ppm relative to TMS (as internal standard) and DMSO$_{d6}$ (centered at 39.50 ppm downfield from TMS), respectively. Coupling constants values are expressed in Hz. ^{13}C chemical shift values were measured from proton fully decoupled spectra. Signals assignment was made on the basis both of known substituent effects and of one-bond multiplicities (indicated in parentheses) determined by DEPT-135. Mass spectra (EI) were collected on a GC-MS-QP5050A Shimadzu mass spectrometer with ionization energy (EI) of 70 eV. Elemental analyses were performed on a Perkin–Elmer 240 8C elemental analyzer and the results were within ±0.4% of the theoretical values. Yields of compounds refer to purified products and are not optimized.

Analytical and spectroscopic data for starting material o-nitro-phenyl-triketone **1** together with o-nitrophenyl-pyrrole **2** and o-amino-phenyl-pyrrole **3** were prepared according to previous procedures reported by us [14].

5.1.1. General procedure for the preparation of PQs (4g-i)

To a solution of (2-amino-phenyl)-pyrrole **3** (0.57 mmol), in dry DMF (5 ml), the suitable aldehyde (0.63 mmol) and catalytic amount of p-TsOH (15 mol%) were added. Initially, the mixture was stirred, at r.t. for 10 min and after, under heating at 100 °C for 3 h. When the reaction was judged complete (TLC monitoring), the mixture was allowed to reach room temperature. Evaporation of the solvent under reduced pressure gave rise a dark residue which was dissolved in dichloromethane (30 ml) and washed with 3 × 10 ml of 5% aqueous NaHCO3 solution. The organic extracts dried with MgSO4 and evaporated in vacuo afforded a dark solid which was purified by column chromatography (eluant DCM/AcOEt 9:1).

5.1.1.1. 3-Acetyl-4-(benzo[d] [1,3]dioxol-5-yl)-2-methyl-1H-pyrrolo[3,2-c]quinoline (4g).
This compound was obtained by treatment of **3** with benzo[d] [1,3]dioxole-5-carbaldehyde for 3 h. Recrystallization from

EtOH yielded 70% of brown solid powder; mp: 229–330 °C; IR: cm^{-1}: 3244 broad (NH), 1643 (CO); ^{1}H NMR (400 MHz, DMSO) δ 12.82 (s, 1H, NH), 8.37 (dd, J = 6.9, 2.5 Hz, 1H, CH), 8.03 (dd, J = 7.2, 2.3 Hz, 1H, CH), 7.67–7.56 (m, 2H, CH x2), 7.26 (d, J = 1.6 Hz, 1H, CH), 7.14 (dd, J = 8.0, 1.7 Hz, 1H, CH), 7.02 (d, J = 8.0 Hz, 1H, CH), 6.12 (s, 2H, CH$_2$), 2.55 (s, 3H, CH$_3$), 1.75 (s, 3H, CH$_3$). ^{13}C NMR (101 MHz, DMSO) δ 197.19, 153.43, 148.19, 148.09, 143.62, 139.18, 136.73, 135.69, 132.71, 129.59, 127.53, 126.17, 122.85, 121.21, 118.15, 116.48, 109.03, 108.68, 101.80, 31.88, 13.23. GC-MS: m/z: 75 (5.9%), 94 (3.5), 108 (12.9), 121 (33.9), 128 (10.8), 135 (11.7), 143 (9.5), 164 (7.8), 172 (9.6), 243 (23.1), 255 (4.5), 271 (16.2), 285 (4.2), 301 (9.3), 315 (12.1), 329 (100), 344 (77.3). Anal. Calculated for C$_{21}$H$_{16}$N$_2$O$_3$, Mol. Wt.: 344, 4: C, 73,24; H, 4,68; N, 8,13; Found: C, 73,47; H, 4,65; N, 8,16.

5.1.1.2. 3-Acetyl-4-(4-bromobenzo[d] [1,3]dioxol-5-yl)-2-methyl-1H-pyrrolo[3,2-c]quinoline (4h).

This compound was obtained by treatment of **3** with 4-bromo-benzo[d] [1,3]dioxole-5-carbaldehyde for 3 h. Recrystallization from ethanol yielded 72% of light brown solid. Recrystallised from EtOH, mp: 229–230 °C with decomposition; IR: cm^{-1}: 3195 (NH), 1644 (CO); ^{1}H NMR (200 MHz, DMSO) δ 12.84 (s, 1H, NH), 8.42 (dd, J = 2.8, 4.9, 1H, CH), 8.03 (dd, J = 2.7, 5.4, 1H, CH), 7.65 (dd, J = 3.1, 6.3, 2H, CH x2), 7.29 (s,1H, CH), 7.05 (1H, s, CH), 6.16 (d, J = 8.4, 2H, CH$_2$), 2.61 (s, 3H, CH$_3$), 1.95 (s, 3H, CH$_3$). ^{13}C NMR (50 MHz, DMSO) δ 195.26 (s), 152.85 (s), 147.97(s), 147.00 (s), 142.59 (s), 139.58 (s), 136.25 (s), 134.67 (s), 129.18 (d), 127.10 (d), 126.26 (d), 120.79 (d), 117.85 (s), 117.10 (s), 116.19 (s), 112.79 (s), 112.03 (d), 110.77 (d), 102.14 (t), 30.45 (q), 13.57 (q). GC-MS: m/z M+ 422/424 8.5%), 391 (1.2), 343 (1.3), 330 (1.4), 315 (5.1), 287 (13.3), 266 (100), 237 (7.8), 208 (9.8), 150 (42.9), 133 (41.6), 104 (8.4), 133 (41.6), 104 (8.4), 86 (6.9), 75 (21.1). Anal. Calculated for C$_{21}$H$_{15}$BrN$_2$O$_3$, mol. Wt.: 423.3: C, 59,59; H, 3.57; N, 6.62; found: C, 59,36; H, 3.59; N, 5.59

5.1.1.3. 3-Acetyl-4-(2-hidroxyl-3,5-dichlorophenyl)-2-methyl-1H-pirrolo[3,2-c]quinoline (4i).

This compound was obtained by treatment of **3** with *2-hidroxyl-3,5-dichlorophenyl* carbaldehyde for 3 h. Recrystallization from EtOH yielded 65% of light brown solid powder; mp: 299–301 °C; IR: cm^{-1}: 3420 broad (NH and OH), 1642 (CO) cm^{-1}. ^{1}H NMR (200 MHz, DMSO) δ 13.03 (s, 1H, NH), 8.42 (dd, J = 5.4, 3.1 Hz, 1H, CH), 8. 10 (dd, J = 5.4, 3.1 Hz, 1H, CH), 7.70 (dd, J = 2.7, 5.8, 2H, CH x2), 7.62 (d, J = 1.4, 1H, CH), 7.38 (d, J = 1.4, 1H, CH), 2.65 (s, 3H, CH$_3$), 2.11 (s, 3H, CH$_3$). ^{13}C NMR (50 MHz, DMSO) δ 195.55 (s), 151.77 s), 150.41 (s), 140.92 (s), 140.07 (s), 136.08 (s), 129.43 (d), 128.49 (d), 128.09 (d), 127.90 (d), 126.95 (s), 126.82 (d), 122.08 (s), 121.99 (s), 120.82 (d), 118.13 (s), 116.33 (s), 115.39 (s), 31.31 (q), 13.31 (q). GC-MS: m/z 384 (9%), 366 (100), 351 (36.8), 341 (22.5), 331 (50.2), 303 (16.6), 267 (30.7), 253 (60), 238 (12.3), 151 (21.9), 134 (57.7), 120 (36.9), 106 (21.5), 87 (13), 75 (9.2). Anal. Calculated for C$_{20}$H$_{14}$Cl$_2$N$_2$O$_2$, Mol. Wt.: 385.2: C, 62.35; H, 3.66; N, 7.27; Found: C, 62.47; H, 3.63; N, 7.30.

5.1.2. Method for the synthesis of 5

To a bottom sealed flask conditioned under Argon and cooled in an ice bath, (50 mg 0.14 mmol) of compound **4g** is dissolved in 2 ml of dry DMF. Under stirring, 5 mg of NaH (60% oil dispersion) (0.15 mmol) in 1 mL of Ethyl Ether were added via syringe. A brown solution is formed. After 10 min, via syringe 43 μl of C$_3$H$_6$ClBr (d:1.592) were added dropwise and the mixture were stirred to reach r.t. for 48 h. Quenching with NH$_4$Cl solution and extraction with DCM (3 × 20 ml), gave after evaporation of the solvent, a dark residue which was purified by silica flash column (eluant Petroleum Ether (40–60 °C): Ethyl Acetate 8:2). The first collected fraction gave at the GCMS a m/z a product according to a dehydrohalogenated compound (40%), which was discarded. The second fraction yielded 40% of the expected compound **5**.

5.1.3. 1 3-Acetyl-4-(benzo[d] [1,3] dioxol-5-yl)-1-(chloropropyl)-2-methyl-1H-pyrrolo[3,2-c]quinoline (5)

Recrystallization from EtOH. mp: 164–165 °C; IR) cm^{-1}:1645 (CO^{1}H NMR (200 MHz, CDCl$_3$) δ 8.35 (td, J = 8.1, 1.6 Hz, 2H, CH x2), 7.64 (pd, J = 7.0, 1.6 Hz, 2H, CH x2), 7.38 (d, J = 1.6 Hz, 1H, CH), 7.21 (dd, J = 8.1, 1.8 Hz, 1H, CH), 6.90 (d, J = 8.0 Hz, 1H, CH), 6.04 (s, 2H, CH$_2$), 4.77 (td, J = 7.9, 2.2 Hz, 2H, CH$_2$), 3.65 (dt, J = 23.7, 5.9 Hz, 2H, CH$_2$), 2.91 (d, J = 14.9 Hz, 1H, CH), 2.61 (s, 3H, CH$_3$), 2.54 (m, 1H, CH), 2.48 (dq, J = 14.9, 5.9 Hz, 1H, CH), 1.75 (s, 3H, CH$_3$). ^{13}C NMR (50 MHz, CDCl$_3$) δ 199.75, 191.68, 153.46, 148.62, 148.46, 138.63, 127.28, 126.14, 123.26, 121.06, 120.92, 120.11, 120.04, 118.31, 119.28, 116.94, 116.38, 109.19, 101.38, 41.67, 32.05, 29.54, 28.18, 11.26. GC-MS: m/z M+ 420 (43.2%), M$^+$ +2422 (14.8), 405 (100), 385 (13.8), 344 (8), 329 (8.5), 300, (4), 282 (6.6), 281 (9.2), 253 (9.6), 242 (14.9), 210 (5.7), 191 (3.6), 135 (7.2). Anal. Calculated for C$_{24}$H$_{21}$ClN$_2$O$_3$, Mol. Wt.: 420.9: C, 68.49; H, 5.03; N, 6.66; Found: C, 68.72; H, 4.99; N, 6.60.

5.2. Biology

5.2.1. NCI 60 screening in vitro methodology

NCI 60 Cell One Dose Screen. All compounds selected by NCI 60 Cell screen are tested initially at a single high dose (10^{-5} M) in the full NCI 60 cell panel. Only compounds which satisfy pre-determined threshold inhibition criteria in a minimum number of cell lines will progress to the full 5-dose assay. The threshold inhibition criteria for progression to the 5-dose screen was selected to efficiently capture compounds with antiproliferative activity based on careful analysis of historical DTP screening data. The threshold criteria may be updated as additional data becomes available.

Briefly, cells are seeded in 96 well plates at an appropriate density and incubated for 1 day. After 1 day, some of the plates are processed to determine a time zero density. To the remaining plates, compounds are added over a 5-log M concentration range. Plates are incubated a further 2 days, then fixed and stained with Sulphorhodamine B. Growth inhibition is calculated relative to cells without drug treatment and the time zero control. The use of a time zero control allows the determination of cell kill as well as net growth inhibition. If a particular endpoint falls outside of the testing range for a given cell line, the database assigns a value equal to either the highest or lowest concentration tested. For a potent compound, such that growth inhibition in a given cell line is greater than 50% at all concentrations, the GI$_{50}$ would be imputed to be the lowest concentration tested. For a relatively inactive compound, such that a given cell line was inhibited less than 50% at all concentrations, the GI$_{50}$ is assigned as the highest concentration tested.

In detail, the human tumor cell lines of the cancer screening panel are grown in RPMI 1640 medium containing 5% fetal bovine serum and 2 mM L-glutamine. For a typical screening experiment, cells are inoculated into 96-well microtiter plates in 100 μL at plating densities ranging from 5000 to 40000 cells/well, depending on the doubling time of individual cell lines. After cell inoculation, the microtiter plates are incubated at 37 °C, 5% CO2, 95% air, and 100% relative humidity for 24 h prior to addition of experimental drugs. After 24 h, two plates of each cell line are fixed in situ with TCA, to represent a measurement of the cell population for each cell line at the time of drug addiction (Tz). Experimental drugs are dissolved in DMSO at 400-fold the desired final maximum test concentration and stored frozen prior to use. At the time of drug addition, an aliquot of frozen concentrate is thawed and diluted to twice the desired final maximum test concentration with complete medium containing 50 μg/mL gentamicin.

Following drug addition, the plates are incubated for an additional 48 h at 37 °C, 5% CO2, 95% air, and 100% relative humidity. For adherent cells, the assay is terminated by the addition of cold TCA. Cells are fixed in situ by the gentle addition of 50 μL of cold 50% (w/v) TCA (final concentration, 10% TCA) and incubated for 60 min at 4 °C. The supernatant is discarded, and the plates are washed five times with tap water and air-dried. Sulforhodamine B (SRB) solution (100 μL) at 0.4%

(w/v) in 1% acetic acid is added to each well, and plates are incubated for 10 min at room temperature. After staining, unbound dye is removed by washing five times with 1% acetic acid and the plates are air-dried. Bound stain is subsequently solubilized with 10 mM trizma base, and the absorbance is read on an automated plate reader at a wavelength of 515 nm. For suspension cells, the methodology is the same except that the assay is terminated by fixing settled cells at the bottom of the wells by gently adding 50 μL of 80% TCA (final concentration, 16% TCA). Using the seven absorbance measurements [time zero, (Tz), control growth, (C), and test growth in the presence of drug at the five concentration levels (Ti)], the percentage growth is calculated at each of the drug concentrations levels. Percentage growth inhibition is calculated as

$[(Ti - Tz)/(C - Tz)] \times 100$ for concentrations for which $Ti \geq Tz$ $[(Ti - Tz)/Tz] \times 100$ for concentrations for which $Ti < Tz$

Three dose-response parameters are calculated for each experimental agent. Growth inhibition of 50% (GI_{50}) is calculated from $[(Ti - Tz)/(C - Tz)] \times 100) 50$, which is the drug concentration, resulting in a 50% reduction in the net protein increase (as measured by SRB staining) in control cells during the drug incubation. The drug concentration resulting in total growth inhibition (TGI) is calculated from Ti)Tz. The LC_{50} (concentration of drug resulting in a 50% reduction in the measured protein at the end of the drug treatment as compared to that at the beginning) indicating a net loss of cells following treatment is calculated from $[(Ti - Tz)/Tz] \times 100) -50$. Values are calculated for each of these three parameters if the level of activity is reached; however, if the effect is not reached or is exceeded, the value for that parameter is expressed as greater or less than the maximum or minimum concentration tested.

Adriamycin was tested with each screening run as a quality control measure. This is done to establish the ability of the screen to generate information relevant to mechanism of growth inhibition/cell killing. It is not a reference compound that has unique importance for the compounds [40]. The screening methodology is described in detail at http://dtp.nci.nih.gov/branches/btb/ivclsp.html.

How to interpret the One Dose Data: The One-dose data will be reported as a mean graph of the percent growth of treated cells and will be similar in appearance to mean graphs from the 5-dose assay. The number reported for the One-dose assay is growth relative to the no-drug control, and relative to the time zero number of cells. This allows detection of both growth inhibition (values between 0 and 100) and lethality (values less than 0). For example, a value of 100 means no growth inhibition. A value of 40 would mean 60% growth inhibition. A value of 0 means no net growth over the course of the experiment. A value of −40 would mean 40% lethality. A value of −100 means all cells are dead (from NCI web site).

5.2.2. Cell cultures

Cell lines were grown as adherent monolayers in a humidified ambient (5% air CO2) at 37 °C. Cells were cultured in Eagle's minimum essential medium (MEM) supplemented with heat-deactivated (56 °C, 30 min) 10% FBS, streptomycin and penicillin, 1% nonessential amino acids and 2 mM L-glutamine (all from Euroclone)

5.2.3. MTS assay

Cell proliferation was measured using MTS assay. Cells were seeded in 96-well plates at 2500 cells per well. MTS Reagent (Abcam, ab197010) was added each day and the cells were incubated for additional 3 h. The number of viable cells were determined by the absorbance at 490 nm using SpectraMax M2e Microplate reader (Molecular Devices). An initial absorbance was measured at 6 h after seeding cells, then absorbance was read every 24 h. The experiments were repeated three times and the data represented as the mean of quadruplicate wells ± SD.

5.2.4. Cell treatments

Semiconfluent MCF7 cells were treated with three different concentrations of **4g** (5, 10 and 25 μM) for 72 h. At least three replicates were performed for each experiment.

5.2.5. Cell cycle

Cells were harvested after the treatment and after washing with ice-cold PBS, resuspended at 1×10^6 cells/ml in hypotonic fluorochrome solution (0.1% sodium citrate, 0.03% Nonidet P-40 and 50 μg/ml propidium iodide) for 30 min at room temperature in the dark. For cells acquisition was used FACSCalibur™ flow cytometer, supported by CellQuest acquisition and data analysis software (Becton Dickinson, Mountain View, CA, USA). Cells were identified as M1 (sub-G1 phase), G0/G1 cells as M2, S cells as M3 and G2/M cells as M4, based on DNA content apoptotic. Data were expressed as percentage of cells.

5.2.6. Analysis of intracellular reactive oxygen species (ROS content)

Intracellular ROS were evaluated by flow cytometry using the ROS-sensitive probe 6-carboxy-2′,7′-dichlorodihydrofluorescein diacetate (H2DCFDA, Invitrogen by Thermo Fisher Scientific, C-2938). After treatment, the harvested cells were washed with PBS and stained with 0.5 μM H2DCFDA (30 min, RT in the dark). Cells were rewashed with PBS, and then analyzed by flow cytometric analysis. Data were expressed as percentage of cells.

5.2.7. Clonogenic assay

After stimulation, the cells were collected and seeded out in a six well plate in appropriate dilutions (clonogenic density of 50 cells/cm^2) to form colonies in 1–3 weeks. For as long as necessary for the formation of colonies, the cells were maintained in fresh medium at 37 C in an atmosphere containing 5% CO$_2$. Getting a minimum of 50 cells, colonies were fixed in 100% methanol and later stained with 0.5% crystal violet in 20% methanol. Thus, the plates were air-dried. The colonies were photographed using a digital camera and counted with countPHICS (count and Plot HIstograms of Colony Size) software, a macro written for ImageJ [41]. Data were expressed as colonies number.

5.2.8. Cell counting

Cell cultures, treatments, and cell proliferation assay for MCF-7, MCF-10 and MDA-MB-231. The human non-tumorigenic breast epithelial MCF10A cell line and the human BC MCF7 and MDA-MB-231 cell lines, were purchased from the ATCC company (Manassas, USA) and cultured according to the manufacturer's specifications as previously described [18,19].

The derivative **4g** was added at concentration of 10, 25 and 50 μM to the culture medium of the cells seeded in 24-well plates the day before treatments and incubated for 24 h. At this time point, cell proliferation assay by cell counting with a Countess Automated Cell Counter and Burker camera according manufacturer's instructions (Invitrogen, Carlsbad, CA, USA) was performed as previously reported [18]. In addition, after 24 h, the medium was changed in order to remove the derivative **4g** to other cell samples which were left to grow in culture for up to 72 h after treatment and then cell counting was performed as described above. The cell growth inhibition values obtained for each cell lines were reported as percentage with respect to the cell number of untreated sample, which was maintained in culture under the same growth conditions in parallel with the treated samples. The data shown were generated from three independent experiments and expressed as the mean ± SD.

5.3. Computational studies

5.3.1. Ligand-based studies

The web-service DRUDIT^{ONLINE} (www.drudit.com) works by four servers, each of which can perform more than ten jobs simultaneously, and several software modules implemented in C and JAVA running on

MacOS Mojave. The Biotarget Finder Module was used to screen small molecule drug candidates as HSP90 and ER inhibitors [26].

5.3.2. Biotarget finder module

The tool provides prediction of the binding affinity between candidate molecules and the specified biological target. The database was uploaded in DRUDIT and submitted to the Biotarget Predictor Tool. The output results were obtained as DAS (Drudit Affinity Score) for each structure, reflecting, the binding affinity of compounds against the HSP90 ATP binding site and the ER Ligand Binding Domain.

5.3.3. Structure-based studies

The preparation process of ligands and protein-ligand complexes used for *in silico* studies has been performed as detailed below:

5.3.4. Ligand preparation

The ligands for docking were prepared through the LigPrep tool, available in the Maestro Suite, Schrödinger software [42]. For each ligand, all possible tautomers and stereoisomers were generated for a pH of 7.0 ± 0.4, using default setting, through the Epik ionization method [42]. Consequently, the integrated Optimized Potentials for Liquid Simulations (OPLS) 2005 force field was used to minimize the energy status of the ligands [43]. The co-crystalized ligands (PubChem CID 124220253 and 6852176, for PDB ID 5GGZ [27] and 2EWP [28], respectively) were prepared using the same tool.

5.3.5. Protein preparations

The high-resolution crystal structure of HSP90 (PDB ID: 5GGZ) [27] and ER (PDB ID: 2EWP) [28] were downloaded from the Protein Data Bank [44]. Both the two protein structures were prepared using the Protein Preparation Wizard, in the Schrödinger software, with the default setting [42]. In detail, bond orders were assigned, including Het group, hydrogen atoms were added, all water molecules were delated, and protonation of the heteroatom states were carried out using the Epik-tool (with the pH set at biologically relevant values, i.e., at 7.0 ± 0.4). The H-bond network was then optimized. The structure was finally subjected to a restrained energy minimization step (RMSD of the atom displacement for terminating the minimization was 0.3 Å), using the OPLS 2005 force field [45].

5.3.6. Docking validation

Molecular Docking studies were executed and scored by using the Glide module, available in the Schrödinger Suite program package. The receptor grids were obtained through assignment the original ligands as the centroid of the grid boxes. The generated 3D conformers were docked into the receptor model using the Extra Precision (XP) mode as the scoring function. A total of 5 poses per ligand conformer were included in the post-docking minimization step, and a maximum of 2 docking poses were generated for each ligand conformer. The proposed docking procedure was able to re-dock the original ligands (PubChem CID 124220253 and 6852176, for PDB ID 5GGZ [27] and 2EWP [28], respectively) within the receptor-binding pockets with RMSD <0.51 Å and docking scores of −8.803 and −13.621, respectively.

5.3.7. Induced Fit Docking

Induced Fit Docking simulations were performed using the IFD application, an accurate and robust Schrödinger technology that accounts for both ligand and receptor flexibility [46,47]. Schrödinger's Induced Fit Docking validated protocol was applied by using HSP90 and ER proteins from the Protein Data Bank (PDB IDs 5GGZ [27] and 2EWP) [28], previously refined by the Protein Preparation module. The IFD score (IFD score = 1.0 Glide Gscore + 0.05 Prime Energy), which includes protein-ligand interaction energy and system total energy, was calculated, and used to rank the IFD poses. The more positive in modulus was the IFD score, the more favorable was the binding.

Declaration of competing interest

The authors declare that they have no known competing financial interests or personal relationships that could have appeared to influence the work reported in this paper

Data availability

Data will be made available on request.

Appendix A. Supplementary data

Supplementary data to this article can be found online at https://doi.org/10.1016/j.ejmech.2023.115537.

References

[1] G.C. Wright, E.J. Watson, F.F. Ebetino, G. Lougheed, B.F. Stevenson, A. Winterstein, Synthesis and hypotensive properties of new 4-aminoquinolines, J. Med. Chem. 14 (1971) 1060–1061, https://doi.org/10.1021/jm00293a010. PMID: 5115204.

[2] F. Heidempergher, P. Pevarello, A. Pillan, V. Pinciroli, A. Della Torre, C. Speciale, M. Marconi, M. Cini, S. Toma, F. Greco, M. Varasi, Pyrrolo[3,2-c]quinoline derivatives: a new class of kynurenine-3-hydroxylase inhibitors, Farmaco 54 (3) (1999) 152–160, https://doi.org/10.1016/S0014-827X(99)00009-9. PMID: 10371028.

[3] J.M. Shin, G. Sachs, Proton pump inhibitors and acid pump antagonists, in: S. Offermanns, W. Rosenthal (Eds.), Encyclopedia of Molecular Pharmacology, Springer, Berlin, Heidelberg, 2008, https://doi.org/10.1007/978-3-540-38918-7_127 . Print ISBN978-3-540-38916-3. Online ISBN978-3-540-38918-7.

[4] P. Jeffrey Conn; Craig W. Lindsley, Hopkins, Corey R. Hopkins, Brian A. Chauder, Rocco D. Gogliotti, Michael R. Wood, Substituted 1H-pyrrolo[3,2-c]quinolin-4(5h)-one analogs as positive allosteric modulators of the muscarinic acetylcholine receptor m4. Application PCT/US2012/036925 events. WO2012154731A1. WIPO (PCT). https://patents.google.com/patent/WO2012154731A1 https://patentscope.wipo.int/search/en/detail.jsf?docId=WO2012154731.

[5] P.H. Beck, M.B. Brown, D.E. Clark, A. Coates, Dyke, J. Hazel, Y. Hu, D.J. Londesbrough, K. Mills, T.D. Pallin, G.P. Reid, G. Stoddart, Preparation of pyrrolo[3,2-c]quinoline derivatives useful in prepn. of medicaments for treatment and prevention of microbial infections by killing clin. latent microorganisms, PCT Int. Appl. (2007) 179 pp. CODEN: PIXXD2 WO 2007054693 A1 20070518 CAN 146:521780 AN 2007:538400.

[6] G. Höfle, B. Böhlendorf, T. Fecker, F. Sasse, B. Kunze, Semisynthesis and antiplasmodial activity of the quinoline alkaloid aurachin, J. Nat. Prod. 71 (11) (2008) 1967–1969, https://doi.org/10.1021/np8004612. Epub 2008 Oct 15. PMID: 18922036.

[7] A. R Coates, G. Halls, Y. Hu, Novel classes of antibiotics or more of the same? Br. J. Pharmacol. 163 (2011) 184–194, https://doi.org/10.1111/j.1476-5381.2011.01250.x.

[8] Y. Hu, A.R. Coates, Nonmultiplying bacteria are profoundly tolerant to antibiotics, Handb. Exp. Pharmacol. 211 (2012) 99–119. https://link.springer.com/chapter/10.1007/978-3-642-28951-4_7. PMID: 23090598.

[9] K. Grychowska, G. Satała, T. Kos, A. Partyka, E. Colacino, S. Chaumont-Dubel, X. Bantreil, A. Wesołowska, M. Pawłowski, J. Martinez, P. Marin, G. Subra, A. J. Bojarski, F. Lamaty, P. Popik, P. Zajdel, Novel 1*H*-Pyrrolo[3,2-*c*]quinoline based 5-HT₆ receptor antagonists with potential application for the treatment of cognitive disorders associated with Alzheimer's disease, ACS Chem. Neurosci. 7 (7) (2016) 972–983, https://doi.org/10.1021/acschemneuro.6b00090.

[10] F. Dudouit, R. Houssin, J.P. Hénichart, A Synthesis of new Pyrrolo[3,2-c]quinoline, J. Het. Chem. 38 (2001) 755–758, https://doi.org/10.1002/jhet.5570380335.

[11] T. Ohashi, Y. Oguro, T. Tanaka, Z. Shiokawa, Y. Shibata, Y. Sato, H. Yamakawa, H. Hattori, Y. Yamamoto, S. Kondo, M. Miyamoto, H. Tojo, A. Baba, S. Sasaki, Discovery of pyrrolo[3,2-c]quinoline-4-one derivatives as novel hedgehog signaling inhibitors, Bioorg. Med. Chem. 15;20 (18) (2012) 5496–5506, https://doi.org/10.1016/j.bmc.2012.07.039.

[12] P. Li, X. Zhang, A.J. Murphy, M. Costa, X. Zhao, H. Sun, Downregulation of hedgehog-interacting protein (HHIP) contributes to hexavalent chromium-induced

malignant transformation of human bronchial epithelial cells, Carcinogenesis 42 (1) (2021) 136–147, https://doi.org/10.1093/carcin/bgaa085.

[13] T. Ohashi, Y. Oguro, T. Tanaka, Z. Shiokawa, Y. Tanaka, S. Shibata, Y. Sato, H. Yamakawa, H. Hattori, Y. Yamamoto, Discovery of the investigational drug TAK-441, a pyrrolo[3,2-c]pyridine derivative, as a highly potent and orally active hedgehog signaling inhibitor: modification of the core, Bioorg. Med. Chem. 20 (18) (2012) 5507–5517, https://doi.org/10.1016/j.bmc.2012.07.034.

[14] M.L. Testa, L. Lamartina, F. Mingoia, A new entry to the substituted pyrrolo[3,2-c] quinoline derivatives of biological interest by intramolecular heteroannulation of internal imines, Tetrahedron 60 (28) (2004) 5873–5880, https://doi.org/10.1016/j.tet.2004.05.047.

[15] C. Di Sano, C. D'Anna, A. Scurria, C. Lino, M. Pagliaro, R. Ciriminna, E. Pace, Mesoporous silica particles functionalized with newly extracted fish oil (Omeg@ Silica) inhibit lung cancer cell growth, Nanomedicine 16 (23) (2021) 2061–2074, https://doi.org/10.2217/nnm-2021-0202.

[16] D.A. Scudiero, R.H. Shoemaker, K.D. Paull, A. Monks, S. Tierney, T.H. Nofziger, M. J. Currens, D. Seniff, M.R. Boyd, Evaluation of a soluble tetrazolium/formazan assay for cell growth and drug sensitivity in culture using human and other tumor cell lines, Cancer Res. 48 (17) (1988) 4827–4833. https://www.ncbi.nlm.nih.gov/pubmed/3409223. PMID: 3409223.

[17] E.A. Orellana, A.L. Kasinski, B.(S.R.B. Sulforhodamine, Assay in cell culture to investigate cell proliferation, Bio. Protoc. 5;6 (21) (2016), e1984, https://doi.org/10.21769/BioProtoc.1984. PMID: 28573164; PMCID: PMC5448418, https://en.bio-protocol.org/en/bpdetail?id=1984&type=0.

[18] L. Minafra, N. Porcino, V. Bravatà, D. Gaglio, M. Bonanomi, E. Amore, F. P. Cammarata, G. Russo, C. Militello, G. Savoca, M. Baglio, B. Abbate, G. Iacoviello, G. Evangelista, M.C. Gilardi, M.L. Bondì, G.I. Forte, Radiosensitizing effect of curcumin-loaded lipid nanoparticles in breast cancer cells, Sci. Rep. 9 (1) (2019), 11134, https://doi.org/10.1038/s41598-019-47553-2.

[19] L. Minafra, V. Bravatà, F.P. Cammarata, G. Russo, M.C. Gilardi, G.I. Forte, Radiation gene-expression signatures in primary breast cancer cells, Anticancer Res. 38 (5) (2018) 2707–2715, https://doi.org/10.21873/anticanres.12512. PMID: 29715090.

[20] K. Ikeda, S. Inoue, Estrogen receptors and their downstream targets in cancer, Arch. Histol. Cytol. 67 (5) (2004) 435–442, https://doi.org/10.1679/aohc.67.435. PMID: 15781984.

[21] E.A. Ariazi, V.C. Jordan, Estrogen-related receptors as emerging targets in cancer and metabolic disorders, Curr. Top. Med. Chem. 6 (3) (2006) 203–215, https://doi.org/10.2174/156802661006030203. PMID: 16515477.

[22] J.M. Holzbeierlein, A. Windsperger, G. Vielhauer, Hsp90: a drug target? Curr. Oncol. Rep. 12 (2) (2010) 95–101, https://doi.org/10.1007/s11912-010-0086-3. PMID: 20425593.

[23] D. Mahalingam, R. Swords, J.S. Carew, S.T. Nawrocki, K. Bhalla, F.J. Giles, Targeting HSP90 for cancer therapy, Br. J. Cancer 19;100 (10) (2009) 1523–1529, https://doi.org/10.1038/sj.bjc.6605066. Epub 2009 Apr 28. PMID: 19401686; PMCID: PMC2696754.

[24] E.A. Ariazi, J.L. Ariazi, F. Cordera, V.C. Jordan, Estrogen receptors as therapeutic targets in breast cancer, Curr. Top. Med. Chem. 6 (3) (2006) 181–202, https://doi.org/10.2174/156802606776173483. PMID: 16515478.

[25] J. Beliakoff, L. Whitesell, Hsp90: an emerging target for breast cancer therapy, Anti Cancer Drugs 15 (7) (2004) 651–662, https://doi.org/10.1097/01.cad.0000136876.11928.be. PMID: 15269596.

[26] A. Lauria, S. Mannino, C. Gentile, G. Mannino, A. Martorana, D. Peri, DRUDIT: web-based DRUgs DIscovery Tools to design small molecules as modulators of biological targets, Bioinformatics 36 (5) (2020) 1562–1569, https://doi.org/10.1093/bioinformatics/btz783.

[27] F. Jiang, H.J. Wang, Y.H. Jin, Q. Zhang, Z.H. Wang, J.M. Jia, F. Liu, L. Wang, Q. C. Bao, D.D. Li, Q.D. You, X.L. Xu, Novel tetrahydropyrido[4,3-d]pyrimidines as potent inhibitors of chaperone heat Shock protein 90, J. Med. Chem. 8;59 (23) (2016) 10498–10519, https://doi.org/10.1021/acs.jmedchem.6b00912. Epub 2016 Nov 22. PMID: 27933959.

[28] E.Y. Chao, J.L. Collins, S. Gaillard, A.B. Miller, L. Wang, L.A. Orband-Miller, R. T. Nolte, D.P. McDonnell, T.M. Willson, W.J. Zuercher, Structure-guided synthesis of tamoxifen analogs with improved selectivity for the orphan ERRgamma, Bioorg. Med. Chem. Lett. 15;16 (4) (2006) 821–824, https://doi.org/10.1016/j.bmcl.2005.11.030. Epub 2005 Nov 22. PMID: 16307879.

[29] A. Daina, O. Michielin, V. Zoete, SwissADME: a free web tool to evaluate pharmacokinetics, drug-likeness and medicinal chemistry friendliness of small molecules, Sci. Rep. 7 (2017), 42717, https://doi.org/10.1038/srep42717.

[30] J.S. Delaney, ESOL: estimating aqueous solubility directly from molecular structure, J. Chem. Inf. Comput. Sci. 44 (3) (2004) 1000–1005, https://doi.org/10.1021/ci034243x.

[31] J. Ali, P. Camilleri, M.B. Brown, A.J. Hutt, S.B. Kirton, Revisiting the general solubility equation: in silico prediction of aqueous solubility incorporating the effect of topographical polar surface area, J. Chem. Inf. Model. 27;52 (2) (2012) 420–428, https://doi.org/10.1021/ci200387c. Epub 2012 Jan 13. PMID: 22196228.

[32] J.B. Baell, G.A. Holloway, New substructure filters for removal of pan assay interference compounds (PAINS) from screening libraries and for their exclusion in bioassays, J. Med. Chem. 8;53 (7) (2010) 2719–2740, https://doi.org/10.1021/jm901137j. PMID: 20131845.

[33] C.A. Lipinski, F. Lombardo, B.W. Dominy, P.J. Feeney, Experimental and computational approaches to estimate solubility and permeability in drug discovery and development settings, Adv. Drug Deliv. Rev. 1;46 (1–3) (2001) 3–26, https://doi.org/10.1016/S0169-409X(00)00129-0. PMID: 11259830.

[34] D.F. Veber, S.R. Johnson, H.Y. Cheng, B.R. Smith, K.W. Ward, K.D. Kopple, Molecular properties that influence the oral bioavailability of drug candidates, J. Med. Chem. 6;45 (12) (2002) 2615–2623, https://doi.org/10.1021/jm020017n. PMID: 12036371.

[35] W.J. Egan, K.M. Merz Jr., J.J. Baldwin, Prediction of drug absorption using multivariate statistics, J. Med. Chem. 19;43 (21) (2000) 3867–3877, https://doi.org/10.1021/jm000292e. PMID: 11052792.

[36] Y. Sungryul, K. Taemook, H.Y. Kyung, K. Keunsoo, The T47D cell line is an ideal experimental model to elucidate the progesterone-specific effects of a luminal A subtype of breast cancer, Biochem. Biophys. Res. Commun. 486 (3) (2017) 752–758, https://doi.org/10.1016/j.bbrc.2017.03.114.

[37] N.A. Franken, H.M. Rodermond, J. Stap, J. Haveman, C. van Bree, Clonogenic assay of cells in vitro, Nat. Protoc. 1 (5) (2006) 2315–2319, https://doi.org/10.1038/nprot.2006.339. PMID: 17406473.

[38] Y. Xiaodong, Nature protocol, clonogenic assay, Bio-protocol. 2 (10) (2012) e187, https://doi.org/10.21769/BioProtoc.187.

[39] H. Sies, Oxidative stress: a concept in redox biology and medicine, Redox Biol. 4 (2015) 180–183, https://doi.org/10.1016/j.redox.2015.01.002.

[40] S.L. Holbeck, J.M. Collins, J.H. Doroshow, Analysis of Food and Drug Administration-approved anticancer agents in the NCI60 panel of human tumor cell lines, Mol. Cancer Therapeut. 9 (5) (2010) 1451–1460, https://doi.org/10.1158/1535-7163MCT-10-0106.

[41] B. Brzozowska, M. Gałecki, A. Tartas, J. Ginter, U. Kaźmierczak, L. Lundholm, Freeware tool for analysing numbers and sizes of cell colonies, Radiat. Environ. Biophys. 58 (2019) 109–117, https://doi.org/10.1007/s00411-018-00772-z.

[42] G. Madhavi Sastry, M. Adzhigirey, T. Day, R. Annabhimoju, W. Sherman, Protein and ligand preparation: parameters, protocols, and influence on virtual screening enrichments, J. Comput. Aided Mol. Des. 27 (2013) 221–234, https://doi.org/10.1007/s10822-013-9644-8.

[43] J.L. Banks, H.S. Beard, Y. Cao, A.E. Cho, W. Damm, R. Farid, A.K. Felts, T. A. Halgren, D.T. Mainz, J.R. Maple, R. Murphy, D.M. Philipp, M.P. Repasky, L. Y. Zhang, B.J. Berne, R.A. Friesner, E. Gallicchio, R. M Levy, Integrated modeling program, applied chemical theory (IMPACT), J. Comput. Chem. 26 (2005) 1752–1780, https://doi.org/10.1002/jcc.20292.

[44] H. M Berman, J. Westbrook, Z. Feng, G. Gilliland, T.N. Bhat, H. Weissig, I. N. Shindyalov, P.E. Bourne, The protein Data Bank, Nucleic Acids Res. 28 (1) (2000) 235–242, https://doi.org/10.1093/nar/28.1.235.

[45] J.L. Banks, H.S. Beard, Yixiang Cao, E. Art Cho, W. Damm, R. Farid, A.K. Felts, T. A. Halgren, D.T. Mainz, J.R. Maple, R. Murphy, D.M. Philipp, M.P. Repasky, L. Y. Zhang, B.J. Berne, R.A. Friesner, E. Gallicchio, R.M. Levy, Integrated modeling program, applied chemical theory (IMPACT), J. Comput. Chem. 26 (16) (2005) 1752–1780, https://doi.org/10.1002/jcc.20292.

[46] W. Sherman, H.S. Beard, R. Farid, Use of an induced fit receptor structure in virtual screening, Chem. Biol. Drug Des. 67 (1) (2006) 83–84, https://doi.org/10.1111/j.1747-0285.2005.00327.x. PMID: 16492153.

[47] W. Sherman, T. Day, M.P. Jacobson, R.A. Friesner, R. Farid, Novel procedure for modeling ligand/receptor induced fit effects, J. Med. Chem. 49 (2) (2006) 534–553, https://doi.org/10.1021/jm050540c. PMID: 16420040.